Measurement of absorption and charge exchange cross sections in π^+-N scattering

Yasutaka Kanazawa

February 4, 2013

Abstract

In neutrino oscillation study in T2K experiment, the main signal is ($\nu_\ell + n \rightarrow \ell + p$) and background event is ($\nu_\ell + N \rightarrow \ell + N' + \pi$). If produced π is absorbed into nucleus, background event cannot be distinguished from the main signal. However, cross section of π-N interaction has uncertainty of about 30%. This uncertainty is one of large systematic errors. In this thesis, to reduce this systematic error, cross section of π^+ absorption and charge exchange into ^{12}C is measured. 3D scintillating fiber tracker called PIAnO is made to measure absorption and charge exchange events using π^+ beam in TRIUMF. Data are taken in 2010 and 2011.

In this thesis, beamline, detectors and their performance, MC simulation, reconstruction of tracks and event selections, estimation of systematic error are described. The channel efficiency of PIAnO fiber tracker is measured to be 93.19% (92.90%) in x' (y'). The crosstalk rate of multi-anode PMT in the MC simulation is tuned based on the experimental data. Uncertainty of crosstalk rate is estimated and systematic error of cross section from crosstalk rate is measured to be 0.53%. The total systematic error estimated to be 5.40%.

Cross section of π^+ absorption and charge exchange into ^{12}C is measured to be

$$218.97 \pm 3.7(stat.) - 11.8/ + 10.3(syst.)[mbarn] \quad (1)$$

for 250 MeV/c π^+.

Contents

Chapter 1

Introduction

In T2K experiment, neutrino oscillation with ν_e appearance and ν_μ dis appearance mode is studied. ν_μ beam is made in J-PARC and is detected in Super-Kamiokande. Main signal is charged current quasi elastic interaction ($\nu_\ell + n \to \ell + p$) and background event is ($\nu_\ell + N \to \ell + N + \pi^+$). In background event, sometimes π^+ is absorbed into nucleus, it cannot be distinguished from main signal. However, cross section of π absorption into nucleus has about 20 – 30 % of uncertainty and this becomes one of large systematic error of neutrino oscillation.

In our experiment, cross section of π absorption and charge exchange into nucleus is measured. Data are taken in 2010 (scintillating fiber target of 150 – 375 MeV/c) and 2011 (water target of 200, 275 and 325 MeV/c) in TRIUMF in Canada. Detector called PIAnO is used to select absorption and charge exchange events. PIAnO is made of 1024 scintillating fibers, 32 channels in a layer and 32 layers arranged in orthogonal directions alternately to reconstruct 3D tracks. π-like tracks and proton-like tracks are distinguished by energy deposit of particles. Events without π-like tracks are selected to choose absorption and charge exchange event. In this thesis, detectors, MC simulations, reconstruction and event selections are explained. Channel efficiency of fiber tracker of PIAnO is measured to check detector performance and uncertainty of crosstalk rate of MC is estimated. Then, cross section of π absorption and charge exchange into ^{12}C for 250 MeV/c and its systematic error are measured.

Chapter 2

Physics motivation

2.1 Neutrino oscillation measurements in T2K

In T2K experiment, neutrino oscillation is studied with ν_e appearance and ν_μ disappearance modes using the ν_μ beam produced in J-PARC and Super-Kamiokande detector. The proton beam from the 30GeV synchrotron in J-PARC collides with a carbon target and π^+ is produced. ν_μ from the π^+ decay ($\pi^+ \rightarrow \mu^+ + \nu_\mu$) is used as a beam. ν_μ is detected by ND280 in J-PARC and Super-Kamiokande 295km away. ND280 is shown in Fig. 2.1 and Super-Kamiokande is shown in Fig. 2.2. ND280 detector is made from 5 detectors to measure flux, energy spectrum and cross section of ν_μ beam. Super-Kamiokande is made from 50kt of water tank and PMTs to detect ν_μ and ν_e by Cherenkov light from particles produced in neutrino interaction in water. μ and e can be distinguished by pattern of Cherenkov ring.

The probability of oscillation from ν_μ to ν_e can be approximated as

$$P(\nu_\mu \rightarrow \nu_e) = \sin^2 2\theta_{13} \sin^2 \theta_{23} \sin^2(\frac{1.27\Delta m^2_{13}[eV^2]L[km]}{E_\nu[GeV]}). \quad (2.1)$$

θ_{13} and θ_{23} are mixing angle in MNS (Maki-Nakagawa-Sakata) matrix[1]. Δm^2_{23} is difference of square of mass of neutrinos. L is distance of two detectors. E_ν is the energy of neutrino. To make this probability large, about 0.7 GeV of ν_μ is selected by selecting ν_μ by 2.5 degree from π^+ axis.

The probability for ν_μ to oscillate to other flavors P($\nu_\mu \rightarrow \nu_\alpha$) can be approximated as

$$P(\nu_\mu \rightarrow \nu_\alpha) = \sin^2 2\theta_{23} \sin^2(\frac{1.27\Delta m^2_{23}[eV^2]L[km]}{E_\nu[GeV]}). \quad (2.2)$$

$\sin^2 \theta_{23}$ and Δm^2_{23} are measured from this probability.

For neutrino with $\sim$1GeV energy, the dominant interaction is neutrino-nucleus interaction. Because the properties of neutrinos can be measured only

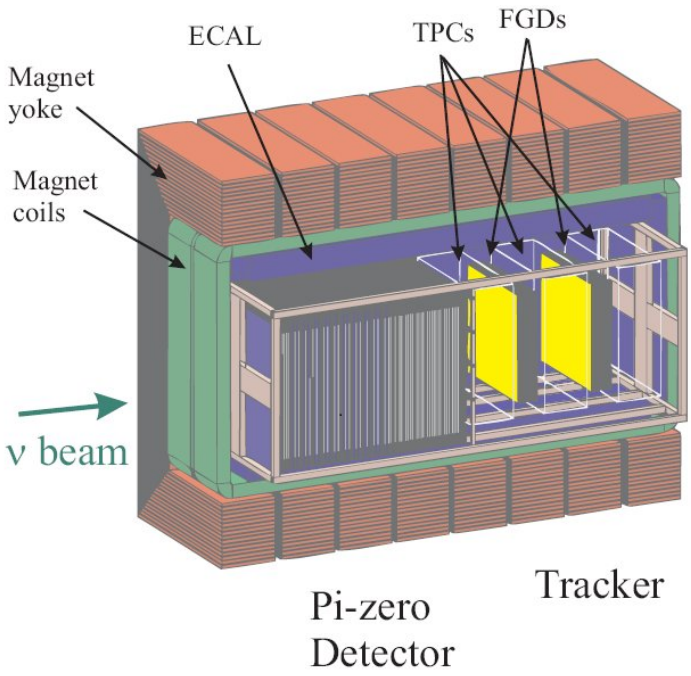

Figure 2.1: ND280

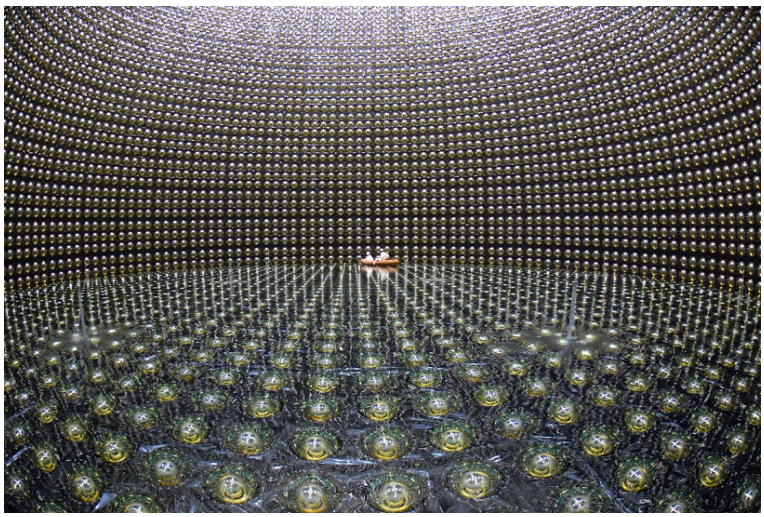

Figure 2.2: Super-Kamiokande

through their interaction, precise knowledge of neutrino interaction is indispensable for neutrino oscillation measurements in T2K. There are several types of neutrino interaction with nucleus. If $W^{\pm}$ is exchanged, it is called charged current interaction. If Z^0 is exchanged, it is called neutral current interaction.

In T2K experiment, the main signal is charged current quasi-elastic interaction ($\nu_\mu + n \rightarrow \mu + p$) because the cross section is the largest for neutrino energy below 1GeV and the neutrino energy can be reconstructed from the final state lepton kinematics. However, there is other types of interaction in which π^+ is produced ($\nu_\mu + N \rightarrow \mu + N + \pi^+$). π^+ created in neutrino-nucleus interaction sometimes interacts with nucleon before going out of nucleus. If π^+ is absorbed into nucleus, π^+ cannot be detected and this event cannot be distinguished from the main signal and gives wrong reconstructed energy. This becomes systematic error of neutrino oscillation measurements. Systematic error of $\sin^2 2\theta_{13} = 0.1$ is shown in Table 2.1. The error of ν_e appearance measurement for $\sin^2 2\theta_{13} = 0.1$ is $\pm 10.3\%$ and the error caused by final state interaction is $\pm 2.4\%$. The understanding of π^+-nucleus interaction is important to reduce the systematic uncertainties in precise measurements of neutrino oscillation in future.

Table 2.1: Systematic error for $\sin^2 2\theta_{13} = 0$

Error source	Systematic error for $sin^2\theta_{13} = 0.1$
Beam flux + ν int. in T2K fit	$\pm 5.7\%$
Final state interaction	$\pm 2.4\%$
ν int. (from other exp.)	$\pm 7.5\%$
Far detector	$\pm 3.1\%$
Total systematic error	$\pm 10.3\%$

2.2 Pion-nucleus interaction

Pion-nucleus interaction is categorized into four types; elastic, inelastic, absorption and charge exchange (CX). If there is π^+ after interaction as shown in Fig. 2.3 and kinetic energy of incident particle is conserved in center of mass frame and ejecting no nuclei and γ rays, it is classified as the elastic event. If there is π^+ after interaction as shown in Fig. 2.4 and kinetic energy of incident particle is not conserved as ejecting nuclei and γ rays, it is classified as the inelastic event. If there is no π^+ and no γ ray from π^0 after interaction as shown in Fig. 2.5, it is classified as absorption event. If there is no π^+ and there is γ ray from π^0 after interaction as shown in Fig. 2.6, it is classified as charge exchange event. In elastic and inelastic events, π^+ exists in the final state. On the other hand, for absorption and charge exchange, there is no π^+ in the final state.

Figure 2.7 shows the cross section of π interaction with ^{12}C with past measurements [2] [3]. Figure 2.8 shows cross section of π interaction with ^{16}O

Figure 2.3: elastic

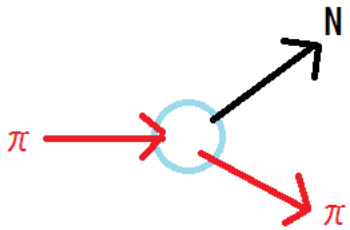

Figure 2.4: inelastic

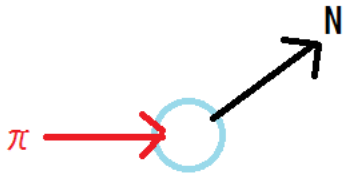

Figure 2.5: absorption

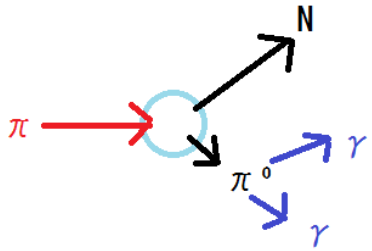

Figure 2.6: charge exchange

with past measurement[4]. In T2K experiment, simulation is tuned by the past data. Lines in Fig. 2.7 and 2.8 are simulation of NEUT [5] [6]. NEUT is made for Kamiodande to simulate neutrino interaction and it is used in Super-Kamiokande, K2K, SciBooNE, T2K. In NEUT, a cascade model is used and probability of interaction is calculated each steps using Δ-hole model until particle going out of nucleus. Model of Salcedo et al. [7] is used for the cross section of π. However, the error of cross section of π^+ absorption and charge exchange into nucleus is about 30%. It becomes one of large systematic error, so reducing those errors are important.

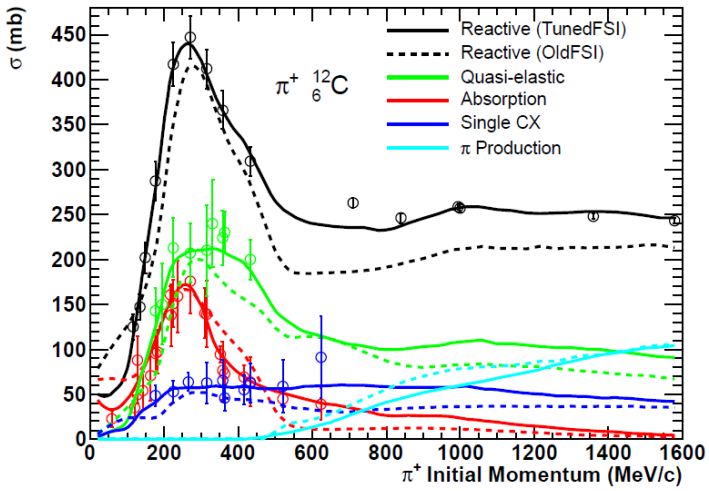

Figure 2.7: Cross section of π interaction with ^{12}C

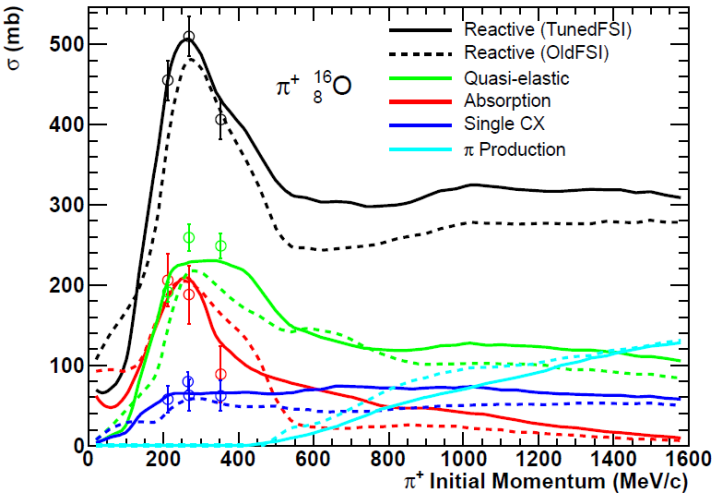

Figure 2.8: Cross section of π interaction with ^{16}O

2.3 Goal of this thesis

We have carried out an experiment to measure the π^+-nucleus interaction cross section. In our experiment, the sum of cross sections of π^+ absorption and charge exchange with ^{12}C is measured by selecting events with no π in the final state. Then, cross section of charge exchange is measured by detecting γ using NaIs. In this thesis, a measurement of the sum of cross section of π^+ absorption and charge exchange with ^{12}C using a scintillating fiber tracker as active target is presented. The goal is to reduce the uncertainty to below 10%.

Chapter 3

Experimental apparatus

In this section, the beamline and detectors are explained.

3.1 TRIUMF M11 beamline

The M11 beamline in TRIUMF in Canada is used. A schematic view of the M11 beamline is shown in Fig. 3.1. Protons from the 500MeV cyclotron collide with a target to produce secondary particles (π, e, μ). The momentum of a particle is selected by a set of slits and magnets. The data was taken in two periods. In 2010 (Run 1), data was taken with a scintillating fiber tracker as a target. In 2011 (Run 2), data was taken with the scintillating tracker interleaved with water.

Table 3.1 shows the list of data taking configurations. In Run 1, the data was taken for the momentum range of 150 – 375 MeV/c with a 25 MeV/c step. In Run 2, the data was taken with 200, 275 and 325 MeV/c. There were two configurations of NaI detector as described in the next section.

Figure 3.1 shows the schematic view of the setup in the experimental area. Figure 3.3 shows the experimental area.

S0 and S1 are plastic scintillators. The size of S0 is 20mm $\times$ 20mm $\times$ 5mm and S1 is 40mm $\times$ 50mm $\times$ 5mm. S0 and S1 are used as trigger. Veto1 and veto2 are 25cm $\times$ 25cm $\times$ 1cm of plastic scintillator. They are used to distinguish events in which particles from the beamline directly hit NaI. In the beam, e and μ are contained in addition to $\pi^{\pm}$. Incident π^{+} is selected by a Cherenkov counter and time of flight (TOF). Cherenkov counter is made from acrylic with refractive index of 1.49. When a particle passes the Cherenkov counter, the signal of Cherenkov counter is different depending on the type of the particle. TOF is measured between a counter in the upstream of the production target and S1. A distribution of Cherenkov vs. TOF for 250MeV/c beam is shown in Fig. 3.4. π^{+} is selected with Cherenkov light and TOF as shown in Fig. 3.4. Purity of π beam for the 250 MeV/c beam is about 99.6% after the selection. List of purity of π beam for each momentum after the selection is shown in

Table 3.1: List of data taking configurations

Run	p(MeV/c)	NaI config	Cherenkov	water	Number of triggers
1	150	1			5M
1	150	2			2.5M
1	200	1			1.5M
1	200	1	in		1.5M
1	200	2			1.5M
1	225	2	in		1.5M
1	250	1			1M
1	250	1	in		1M
1	250	2	in		1.5M
1	275	2	in		1.5M
1	300	1	in		1M
1	300	2	in		1.5M
1	325	1	in		1M
1	325	2	in		1.5M
1	350	1	in		1M
1	350	2	in		1.5M
1	375	2	in		1.0M
1	-200	2			837k
1	-225	2			368k
1	-250	2			380k
2	200	2	in	with	3M
2	200	2	in		3M
2	275	2	in	with	3M
2	275	2	in		3M
2	325	2	in	with	3M
2	325	2	in		3M

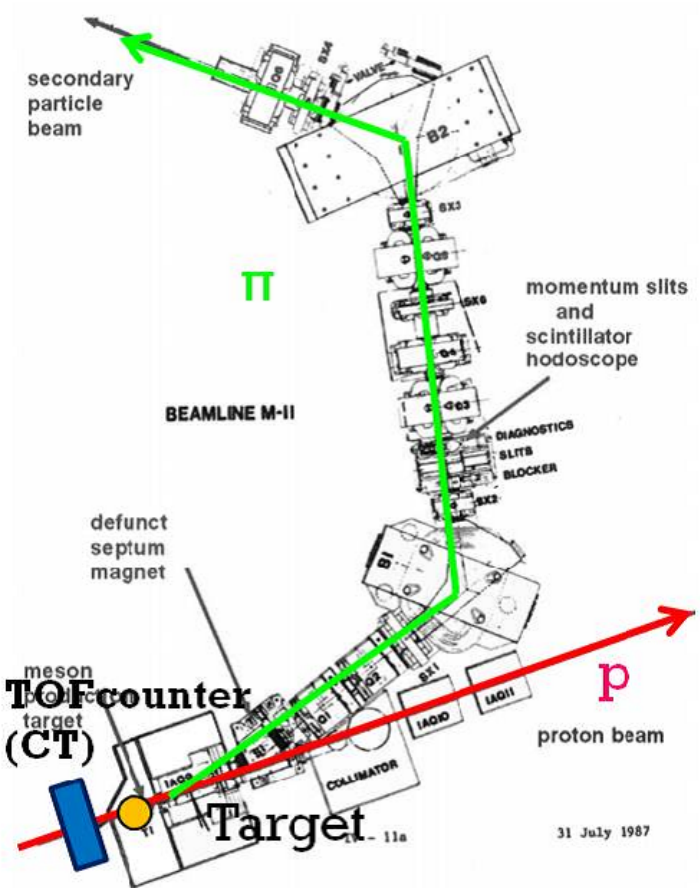

Figure 3.1: Schematic view of M11 beamline

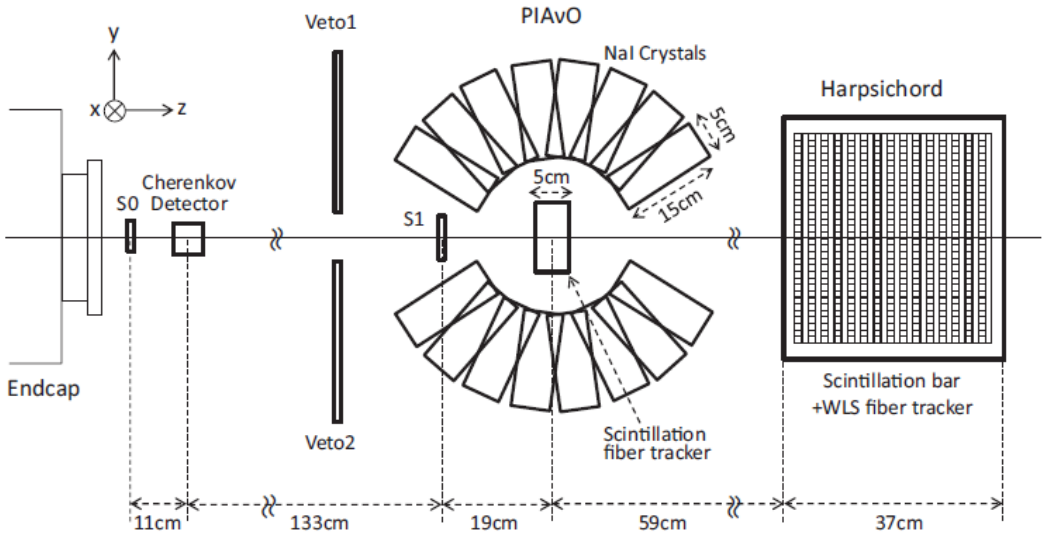

Figure 3.2: Schematic view of the step of the setup in the experimental area

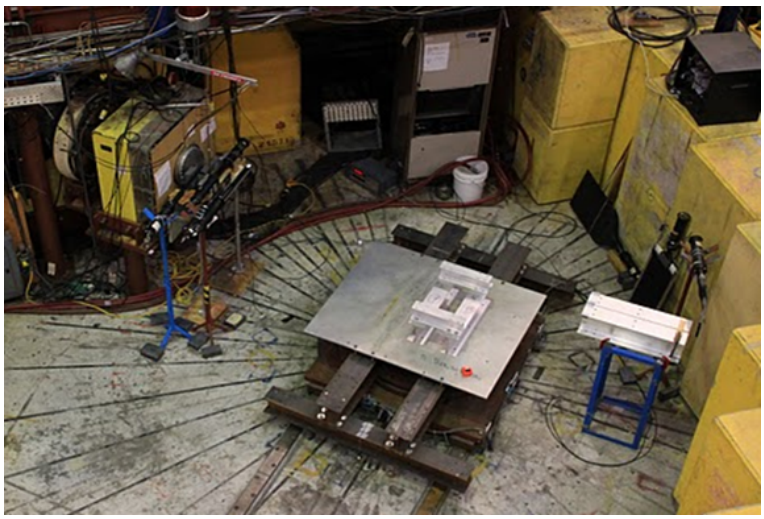

Figure 3.3: The experimental area

Table 3.2.

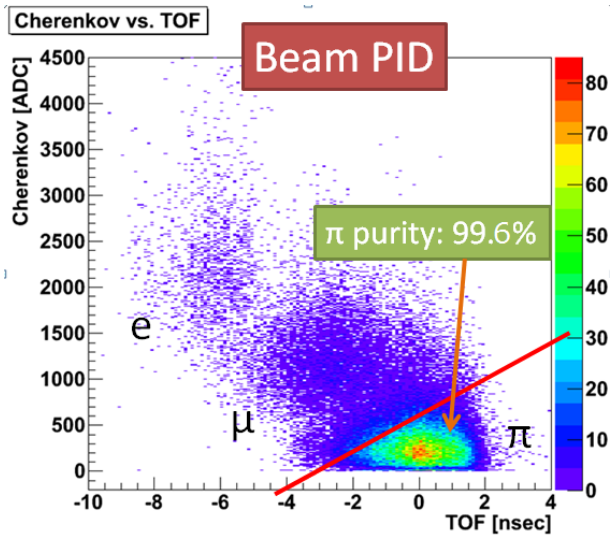

Figure 3.4: Cherenkov vs. TOF for 250MeV/c beam

Table 3.2: Purity of π for each momentum after the selection by Cherenkov counter and TOF

p (MeV/c)	Purity of π beam (%)
200	99.84
225	99.29
250	99.57
275	99.46
300	99.66

3.2 Detector system

Two detectors are used in this experiment; PIAnO and Harpsichord. PIAnO is used to detect the interaction of π^+. Harpsichord is placed downstream of PIAnO and used to detect particles that exit from PIAnO. In this thesis, only data from PIAnO fiber tracker is used for the analysis.

3.2.1 PIAnO (PIon detector for Analysis of ν Oscillation)

The PIAnO detector consists of two parts, a fiber tracker and NaI counters.

The fiber tracker is used as an active target. The NaI counters are placed around the fiber tracker and used to detect γ rays from π^0 decay to identify the charge exchange events. In the fiber tracker, 32 scintillating fibers of 1.5mm $\times$ 1.5mm are grouped to form a layer. Figure of PIAnO fibers is shown in Fig. 3.5. For Run 1, 32 layers are arranged in orthogonal directions alternately. Figure 3.6 shows arrangement of layers in Run1. In Run 2, only 16 layers are used and for half of data taking the fibers are put into water in order to measure the cross section for water target. Layers are staggered by 0.5 channels in order to reduce tracking inefficiency. Fiber configurations for Run 1 and Run 2 are shown in Fig. 3.7 and 3.8, respectively. Layer numbers of Run 1 are defined from most upstream layer to downstream layer as 0 –15 as shown in Fig. 3.7. There are reflecting coating (TiO_2) of 2.5μm thickness on the surface of fibers for optical separation. The whole arrangement of PIAnO is shown in Fig. 3.9. Relation between (x , y) and (x' , y') in PIAnO fiber tracker is shown in Fig. 3.10. There are two coordinate system used in this thesis; (x,y) is used for horizontal and vertical directions. Directions of fibers are rotated by 45° and define (x',y') coordinate.

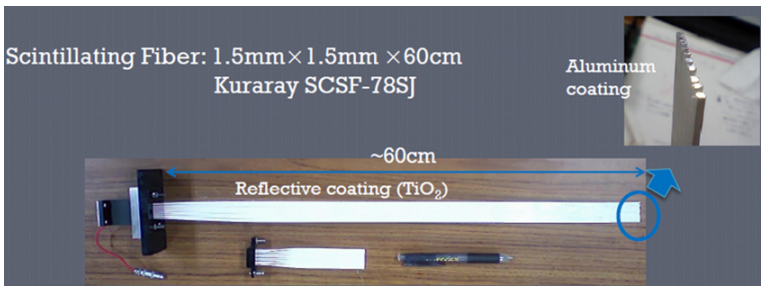

Figure 3.5: PIAnO fibers

Light from a scintillating fiber is detected by a 64 channel multi-anode PMT (MAPMT). MAPMT is shown in Fig. 3.11. The other end of fiber is coated with aluminum in order to increase the light yield. Sixteen MAPMTs are used. Crosstalk is occurred between channels in MAPMT. Crosstalk is a phenomenon that light is leaked and next channel of MAPMT is reacted by mistake. There are two ways happening crosstalk in this experiment. First way is occurred between fibers. Second way is occurred in the surface of MAPMT and light from fiber is leaked to next channel. Second way is occurred about 2%. First way is much less than second way. To reduce effect of crosstalk from reconstruction of track in the fiber tracker, next channels in the fiber tracker is arranged not to be neighboring channel in MAPMT. The charge from MAPMT is recorded using custom electronics[8]. Front end board is shown in Fig. 3.12.

Sixteen NaIs are set around fibers to detect γ rays from π^0. The size of a NaI is 5cm $\times$ 5cm $\times$ 15cm as shown in Fig. 3.13. There are two configurations of position of NaIs as shown in Fig. 3.14. In configuration 1, NaIs are set to

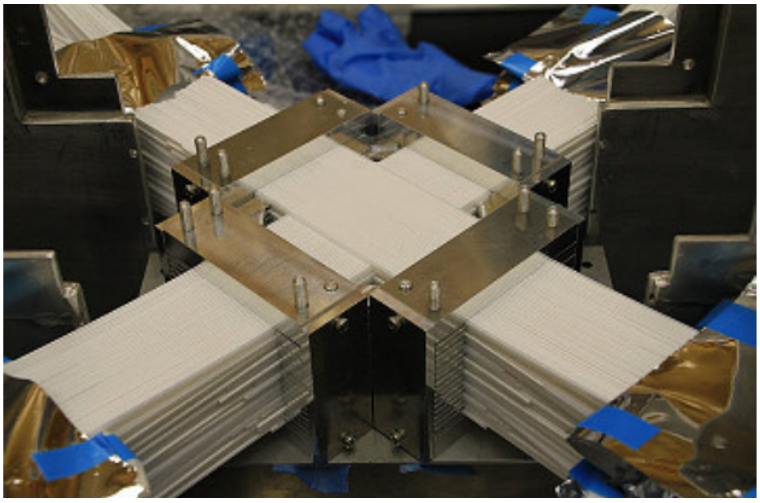

Figure 3.6: Arrangement of layers of fiber in PIAnO

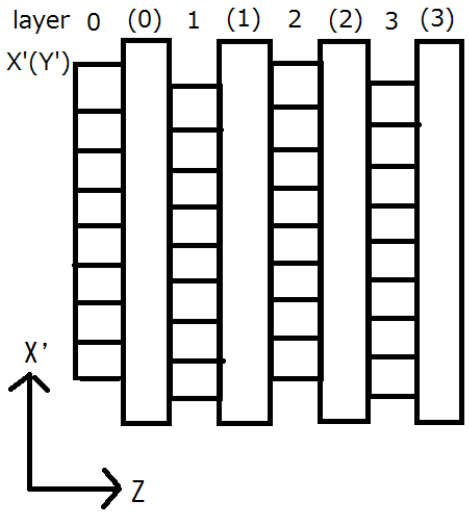

Figure 3.7: Fiber configuration for Run1 and definition of layer numbers

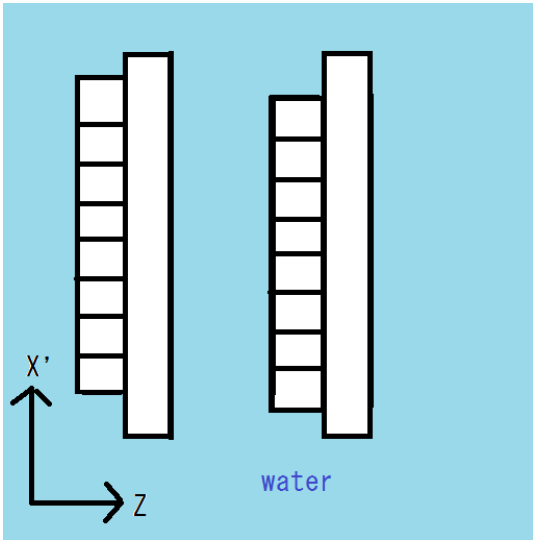

Figure 3.8: Fiber configuration for Run2 (water target)

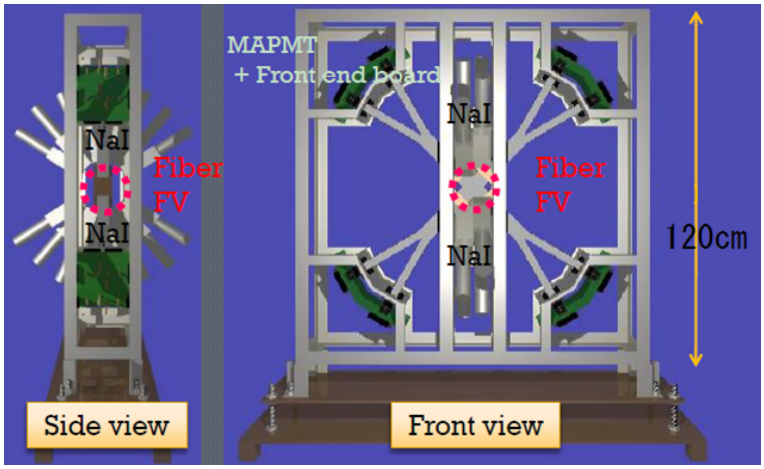

Figure 3.9: PIAnO

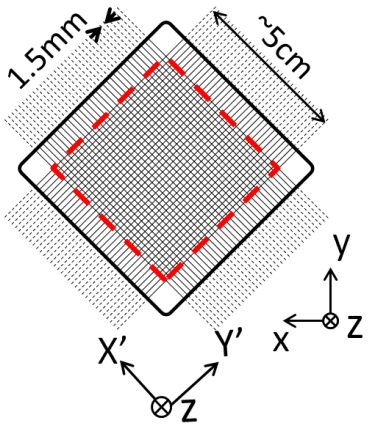

Figure 3.10: Relation between (x , y) and (x' , y')

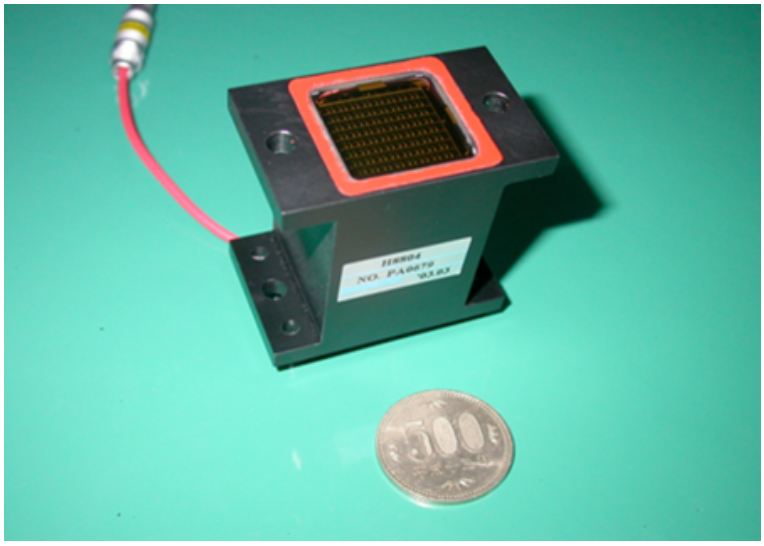

Figure 3.11: MAPMT (Hamamatsu H8804)

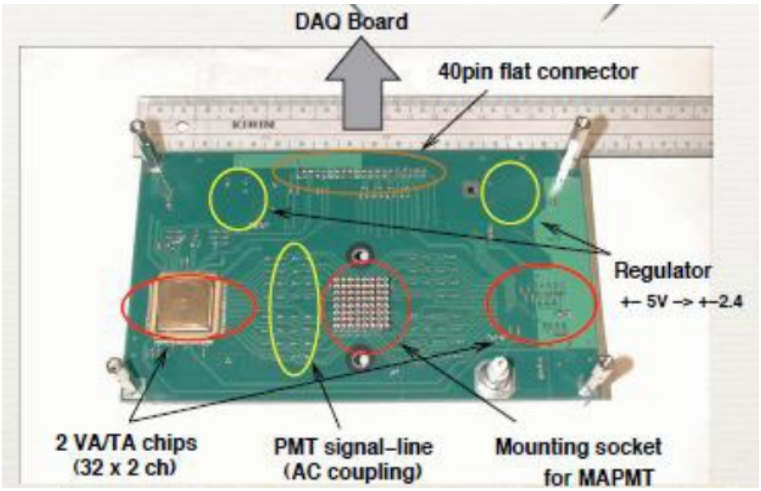

Figure 3.12: Front end board

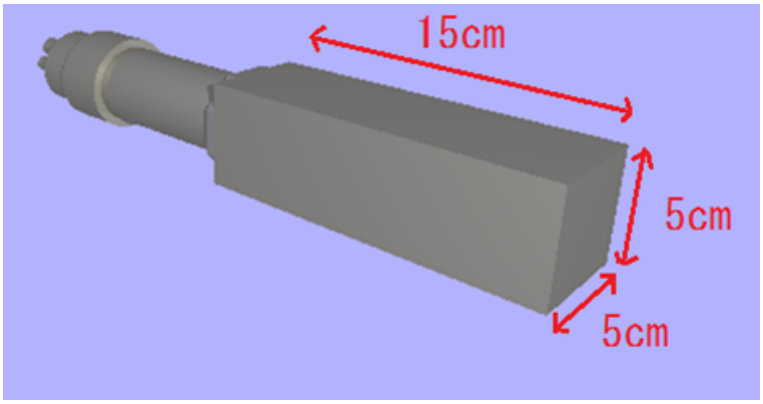

Figure 3.13: NaI

measure the angular distribution of γ rays. In configuration 2, NaIs are set in front of fibers in order to increase the acceptance.

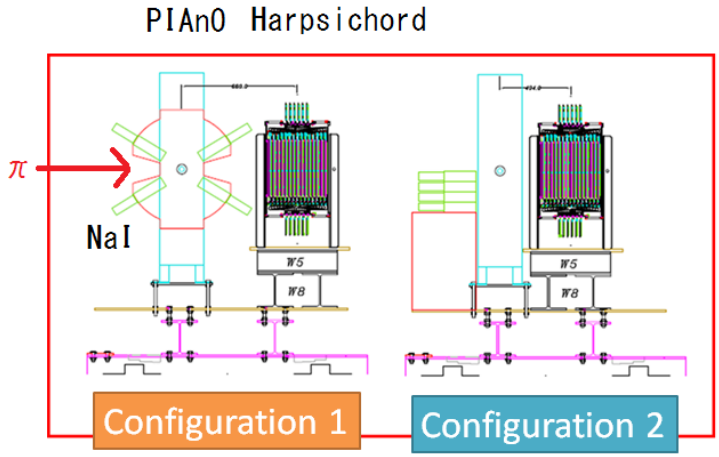

Figure 3.14: Configuration of NaI

3.2.2 Harpsichord

The Harpsichord detector (Fig. 3.15 and 3.16) is constructed using the same detector components as the fine grained detector of the T2K near detector system. In Harpsichord, there are 32 plastic scintillator bars of 1cm $\times$ 1cm in a layer. Thirty layers are set vertically and horizontally. Harpsichord is placed at the most downstream to detect particles exiting from the fiber tracker.

3.3 Monte Carlo simulation (MC)

Geant4 (version9.4.2) is used to simulate physics and detector response. The detailed shapes of detectors are implemented. Charge distribution in MAPMT, π beam profile, crosstalk rate are tuned to the data. Figures 3.17 and 3.18 show beam position of x and angular distribution of y for data and MC simulation.

QGSP_BERT [9] is used in simulation of interaction of π-C. Cross section of elastic of π-C and π-H of past data [2] [10] and default MC of QGSP_BERT is shown in Fig. 3.19. Cross section of elastic scattering of π-C and π-H of MC is tuned to past experiments.

3.3.1 Tuning the crosstalk rate in MC simulation

The crosstalk of MAPMT in the MC simulation is tuned with the real data in the following way. First, tracks going through the detector without interaction

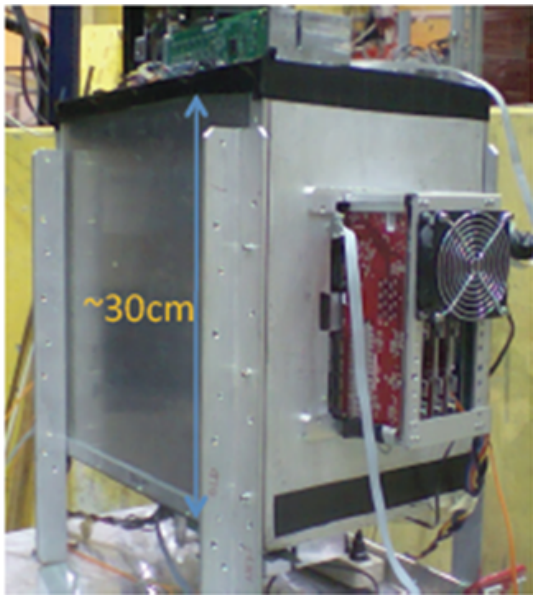

Figure 3.15: Harpsichord

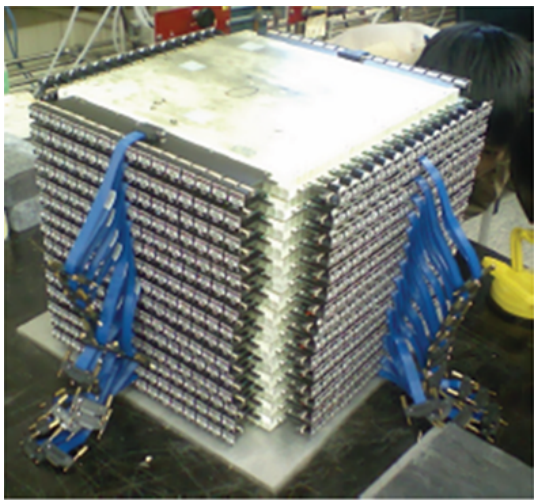

Figure 3.16: Contents of Harpsichord

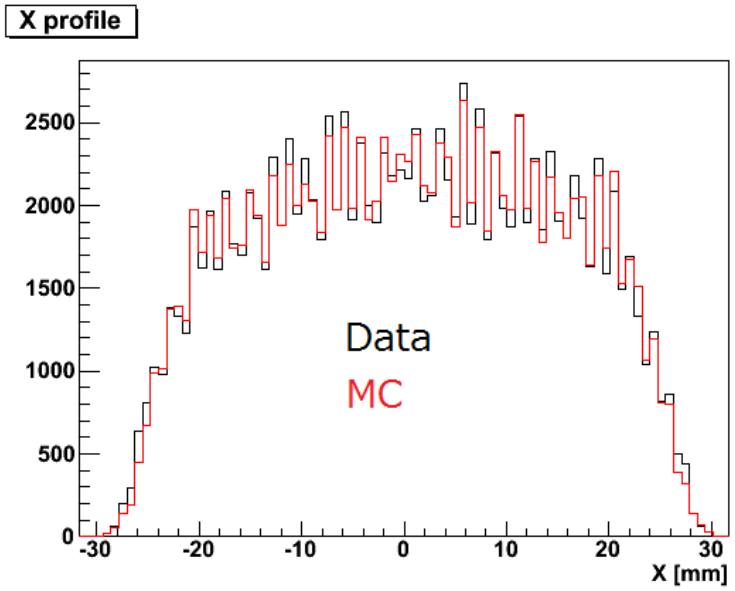

Figure 3.17: Beam position in x

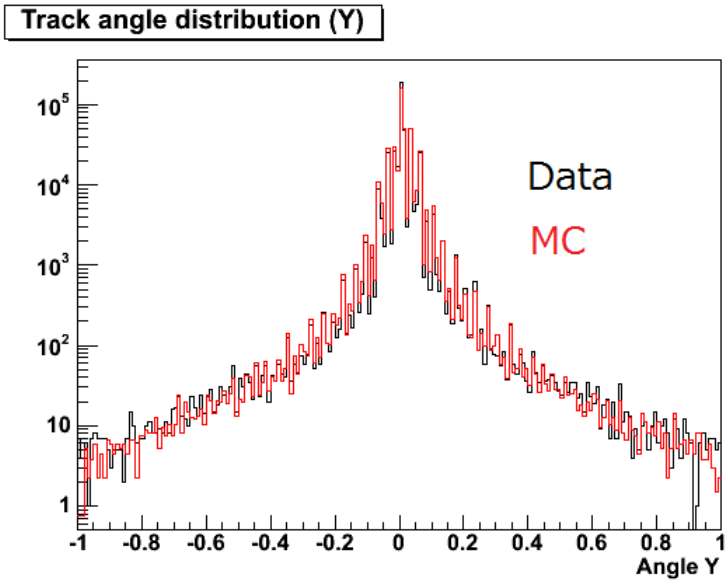

Figure 3.18: Angular distribution of beam in y

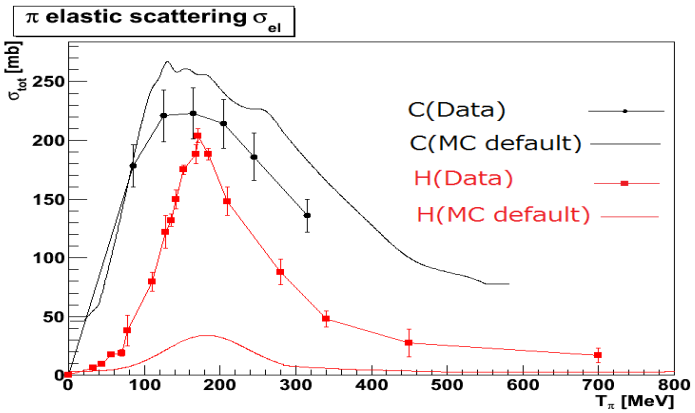

Figure 3.19: Cross section of elastic of π-C and π-H of past data and default MC

and selected. Then, the amount of light by the crosstalk is estimated by looking the light yield of the channels neighboring the track.

The track is reconstructed with the least square method. Hits with more than 5 p.e. and the distance from the reconstructed track within 3/8 channels are selected as the "central channel" in question. If a channel around the central channel in MAPMT has smaller signal than the central channel, it is used to measure the crosstalk and called "crosstalk channel". In order to reject hits with multiple crosstalk effect, if a channel neighboring to the crosstalk channel in MAPMT, other than the central channel, has more 2.5 p.e. or is within 5/8 channels from the track, that crosstalk channel is not used for the crosstalk estimation.

The crosstalk rate is assumed to be identical for all the MAPMT. However, it is known that there is a systematic difference of crosstalk rate depending on the direction of the crosstalk because of misalignment of fixtures to connect fibers and MAPMT. Thus, the crosstalk rate is tuned for each of eight possible positions relative to the central channel. The definition of the channel numbering used in this section is shown in Fig. 3.20. Position of fiber setting to MAPMT slants a little systematically and channel numbering is set to be the same direction. The central channel is numbered as (2,2). All channels with the same number in MAPMT are used together.

The crosstalk rate is independent of the momentum of the particle, while for a lower momentum particle the light yield is higher and the crosstalk effect is easier to measure. Therefore, the real data and MC simulation of 150MeV/c is used for the crosstalk tuning.

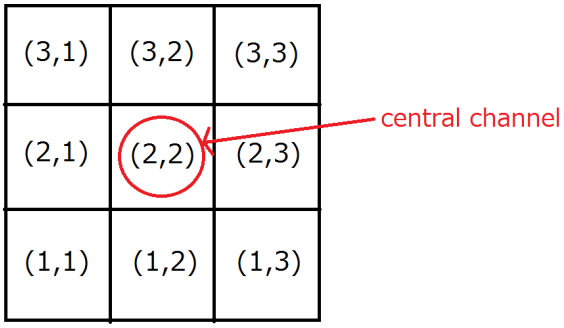

Figure 3.20: Definition of the channel numbering used in this section

Signal of the central channel

Only in this subsection, definition of central channel is changed from 5 p.e. to 2.5 p.e. to show charge distribution over 2.5 p.e. The distributions of the signal for the central channel in data and MC simulation are shown in Fig. 3.21. The average of signal of 2.5 p.e. – 40 p.e. is 17.532 p.e. for data and 17.518 p.e. for MC simulation. The MC simulation agrees with data within the statistical error of 0.2%.

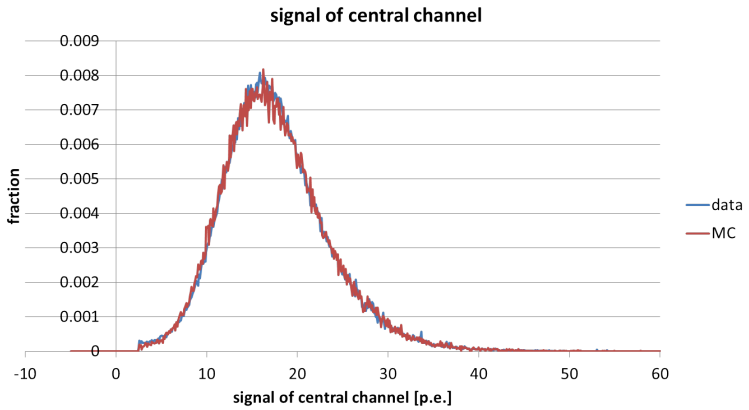

Figure 3.21: Signal of the central channel. Blue (red) histogram shows the distribution for data (MC)

Tuning of the crosstalk rate

The signal of (1,2), (2,1), (2,3), and (3,2) channels are shown in Figs. 3.22, 3.23, 3.24 and 3.25. The crosstalk rate of MC simulation in tuned to reproduce the average in the range of 2.5 p.e. to 5 p.e. in each case.

In order to estimate the uncertainty associated with the crosstalk, the crosstalk rate in the MC simulation is varied and the distribution is compared to the data. In order to take into account the difference of the shape of the distribution, the comparison is done in three regions: 2.5 – 3.0 p.e., 3.0 – 3.5 p.e. and 3.5 – 5.0 p.e. The upper (lower) limit of the crosstalk rate is defined as the crosstalk rate for which the MC value is larger (smaller) than the data by the amount of the statistical uncertainty for all the three regions. Figures 3.26, 3.27, 3.28 and 3.29 show the estimated upper and lower limit of the crosstalk rate for those channels.

A similar procedure is used for the "diagonal" channels ((1,1), (1,3), (3,1) and (3,3)). Because the amount of the crosstalk is smaller, the crosstalk in the MC simulation is tuned by comparing the total MC for 150 MeV/c as shown in Figs. 3.30 – 3.33. Figure 3.34 shows the estimated upper and lower limit of the crosstalk rate for those channels.

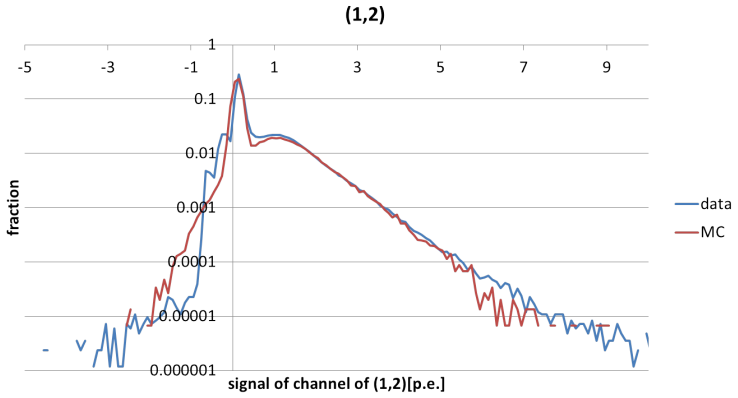

Figure 3.22: Signal of channel of (1,2)

Summary of the crosstalk tuning

The central values, upper and lower limits of the crosstalk in each channel are shown in Tables 3.3, 3.4 and 3.5.

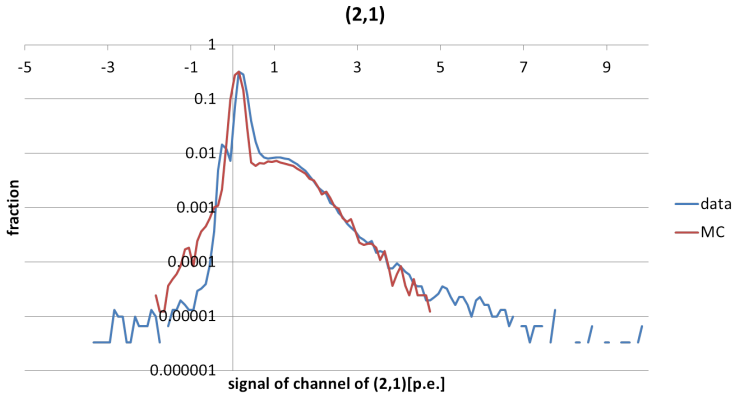

Figure 3.23: Signal of channel of (2,1)

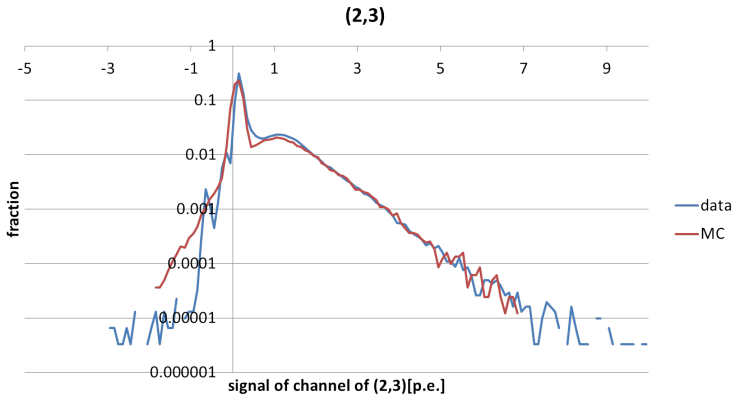

Figure 3.24: Signal of channel of (2,3)

Table 3.3: Estimated central values of crosstalk rate in each channel

(a,b)	$b=1$	2	3
$a=1$	0.15	1.90	0.30
2	0.45	87.12	1.95
3	0.20	0.85	0.15

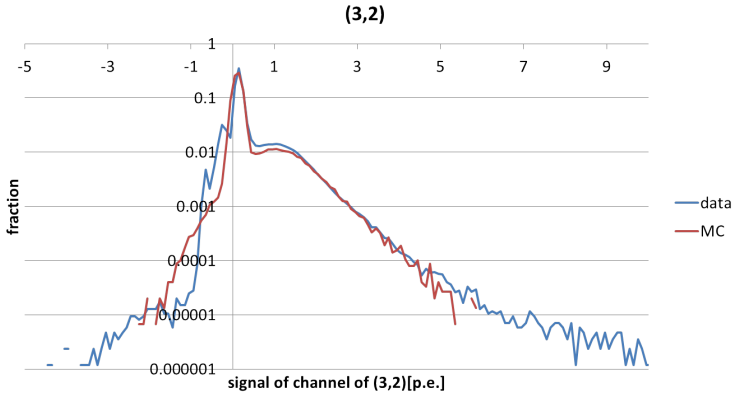

Figure 3.25: Signal of channel of (3,2)

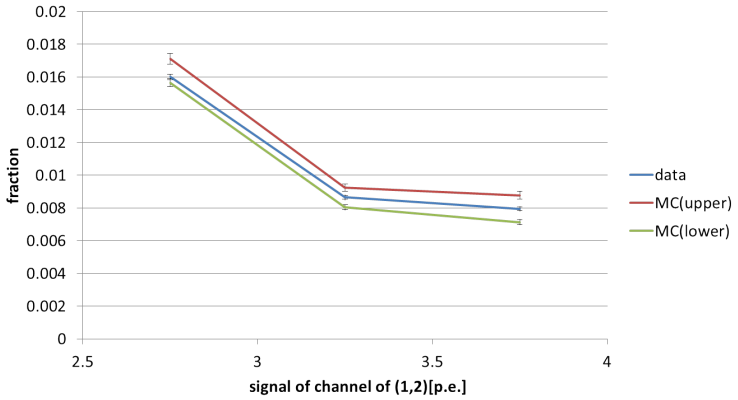

Figure 3.26: Estimated upper and lower limit of crosstalk rate of (1,2)

Table 3.4: Estimated upper limit of the crosstalk rate in each channel

(a,b)	$b=1$	2	3
$a=1$	0.19	1.95	0.39
2	0.55	87.12	2.08
3	0.25	0.96	0.21

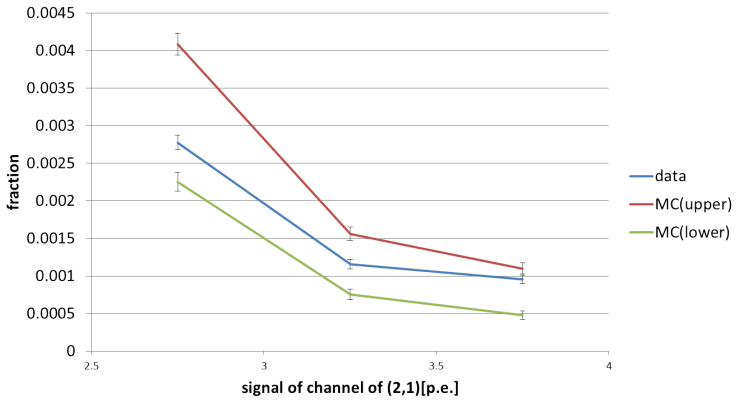

Figure 3.27: Estimated upper and lower limit of crosstalk rate of (2,1)

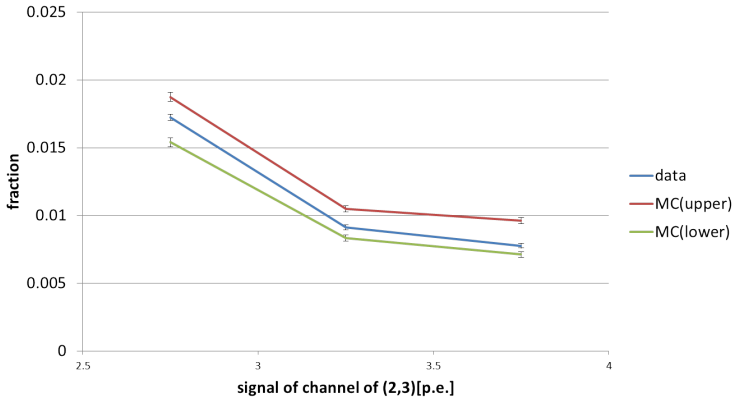

Figure 3.28: Estimated upper and lower limit of crosstalk rate of (2,3)

Table 3.5: Estimated lower limit of crosstalk rate in each channel

(a,b)	$b=1$	2	3
$a=1$	0.22	2.05	0.45
2	0.70	87.12	2.20
3	0.30	1.05	0.25

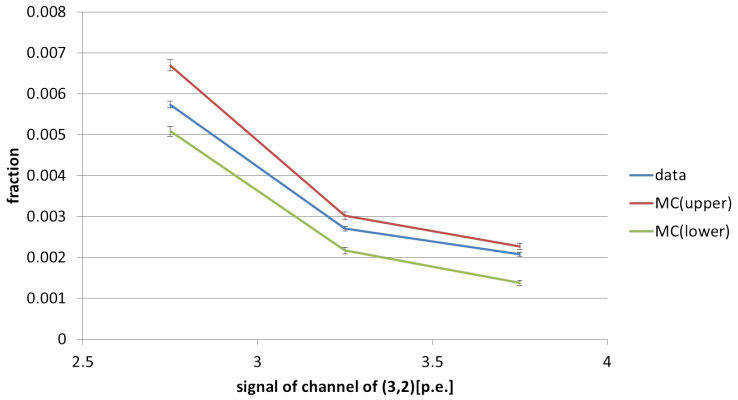

Figure 3.29: Estimated upper and lower limit of crosstalk rate of (3,2)

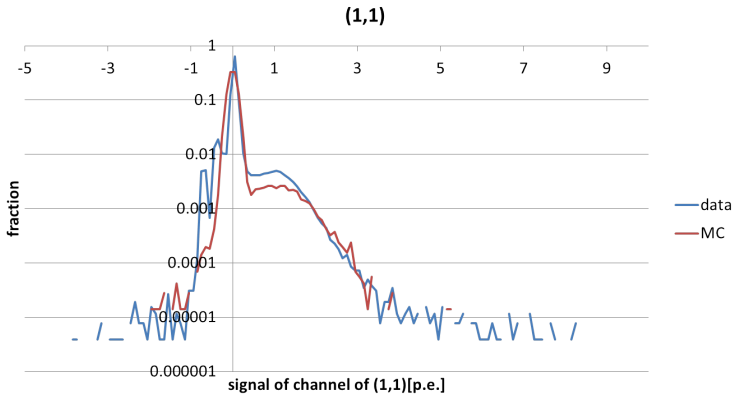

Figure 3.30: Signal of channel of (1,1)

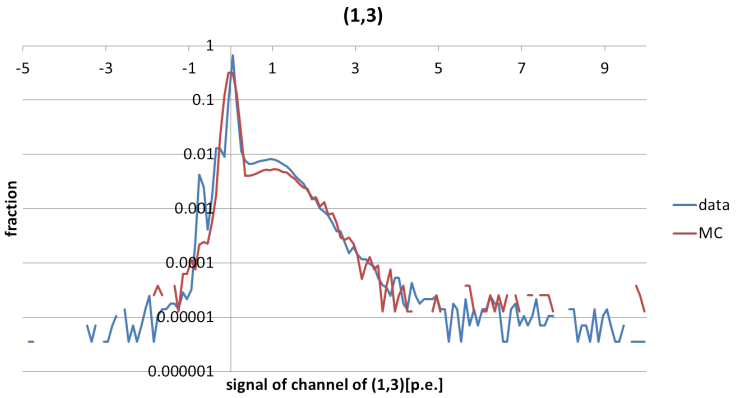

Figure 3.31: Signal of channel of (1,3)

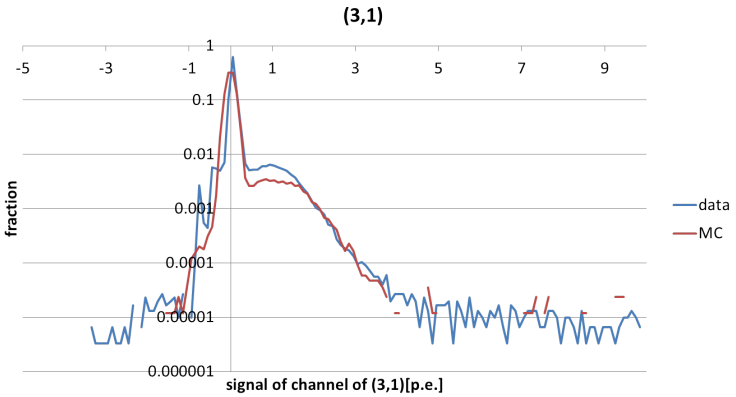

Figure 3.32: Signal of channel of (3,1)

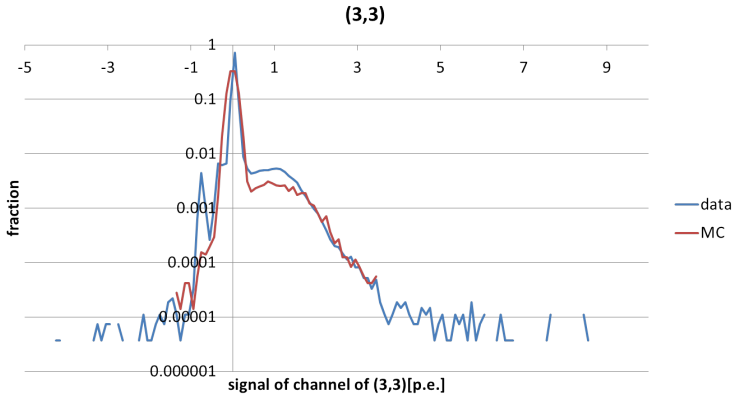

Figure 3.33: Signal of channel of (3,3)

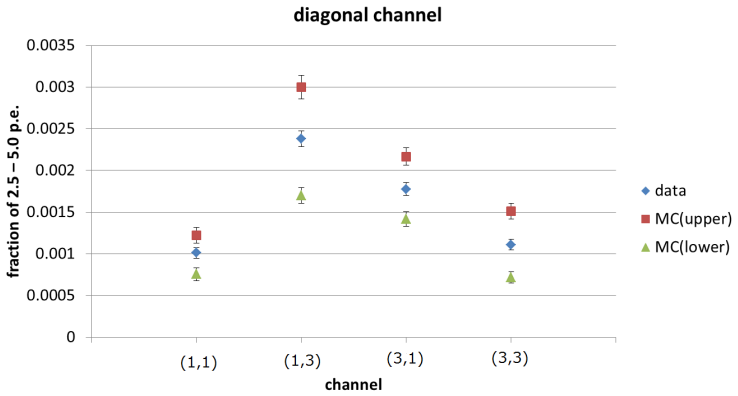

Figure 3.34: Estimated upper limit and lower limit of crosstalk rate of diagonal channel

3.4 Performance of PIAnO fiber tracker

3.4.1 Charge distribution

Charge distributions of signal on a straight track for the real data and MC with 250MeV/c particles are shown in Fig. 3.35. 2.5 p.e. is used as the threshold to define a hit.

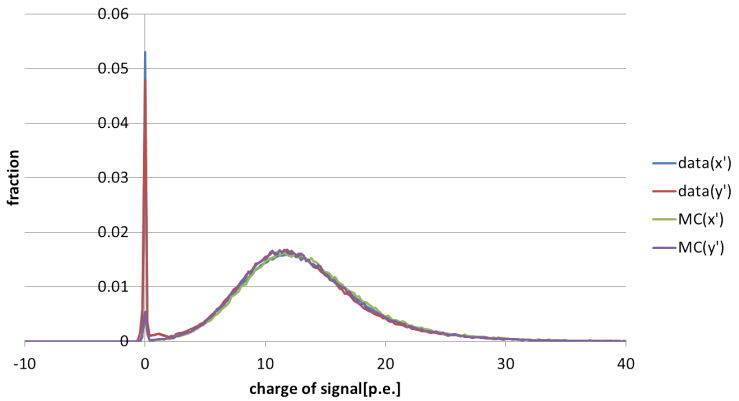

Figure 3.35: Charge distribution of signal on straight track

3.4.2 Channel efficiency of the fiber tracker

The channel efficiency of the fiber tracker is measured. The inefficiency is caused when a particle passes through the gap between fibers or the signal is below 2.5 p.e. threshold.

Figure3.36 is an example of inefficiency channel. Circles show hits with more than 2.5 p.e. and the line shows the reconstructed track.

In order to estimate the channel efficiency, a straight track going through the fiber tracker is selected. Hits are scanned from an upstream layer to the downstream layer. Hits are connected if the position of hit is within 0.5 channels of the hit in the upstream layer. A gap without hits up to two layers is allowed. The angle of track is calculated and a track whose angle θ is $-1/32 < \tan\theta < 1/32$ is selected.

An event display of the through going track is shown in Fig. 3.37 .

The trajectory of a track is calculated with the least square method. Then, hits within ± 1 channel of the calculated trajectory are selected. The channel efficiency is calculated as the ratio of the number of selected hits to the number of hits expected from the reconstructed track for a channel. Layers 14 and 15 are excluded from the calculation because events with interaction may be contained with this method. Data with 250MeV/c beam is used to estimate the channel efficiency.

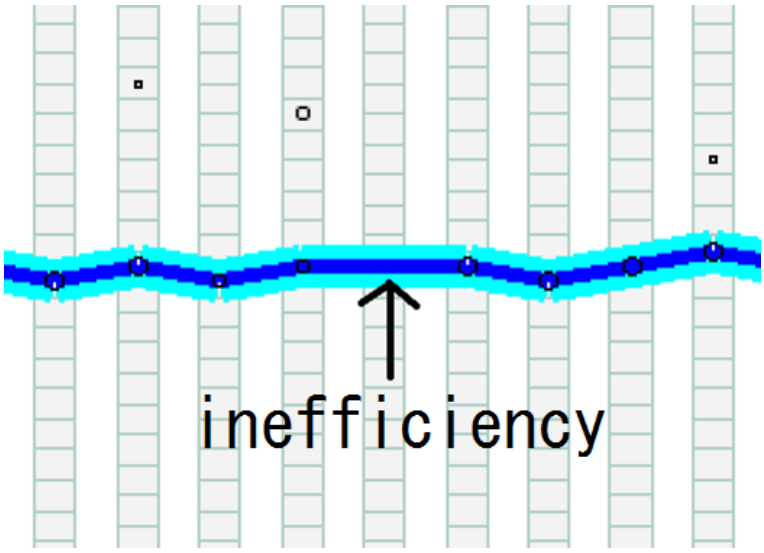

Figure 3.36: Inefficiency channel

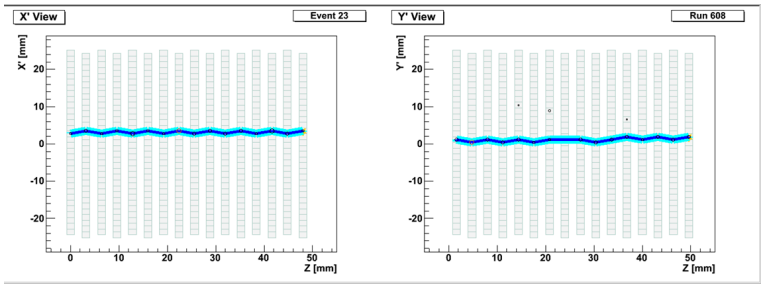

Figure 3.37: An event display of a through going track

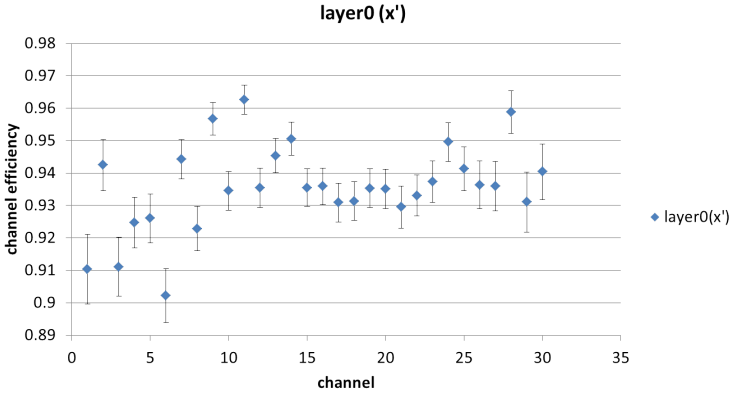

Figure 3.38: Channel efficiency of layer 0 in x'

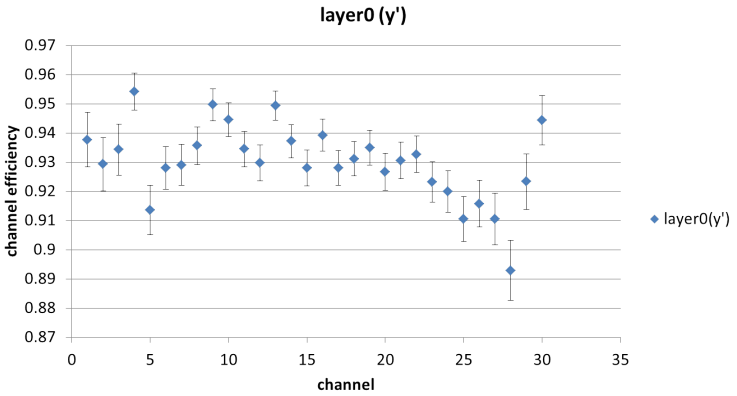

Figure 3.39: Channel efficiency of layer 0 in y'

Figures 3.38 and 3.39 show the channel inefficiency for the layer 0 with statistical error. Efficiency for all channels are shown in Figs. 3.40 and 3.41. Distribution of channel efficiency of x' and y' are shown in Figs. 3.42 and 3.43. The average channel efficiency in x' (y') is 93.19 $\pm$0.04(92.90 $\pm$0.04) % for data. The efficiency for MC is estimated with the same procedure. The average channel efficiency in x' (y') is 93.87 $\pm$0.06(93.77 $\pm$0.06) % for MC simulation.

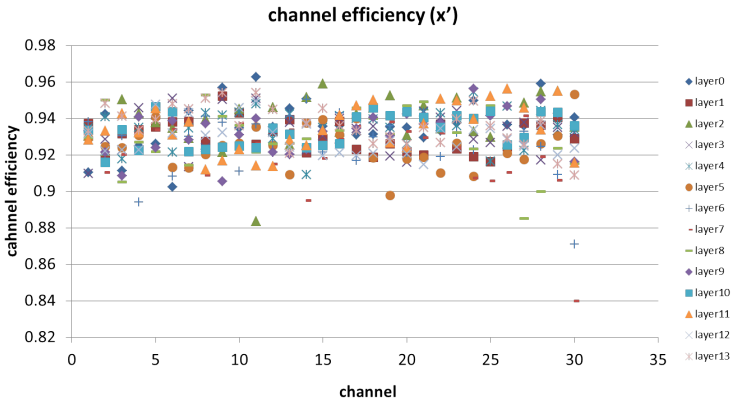

Figure 3.40: Channel efficiency of x'

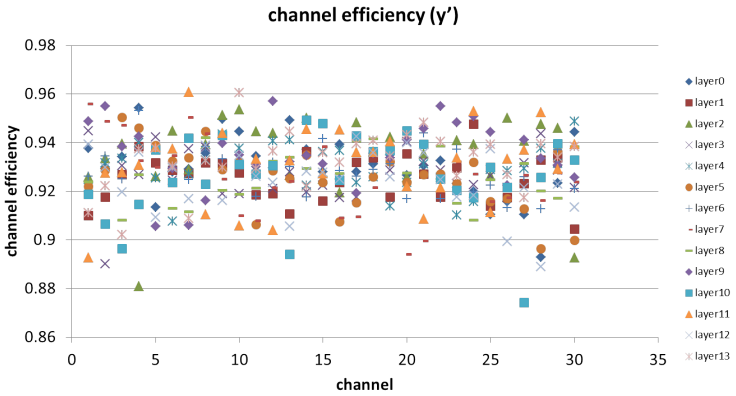

Figure 3.41: Channel efficiency of y'

About 7% of inefficiency is observed. This inefficiency comes from two reasons. First one comes from charge distribution under 2.5 p.e. Second one comes from particle going through gaps between channels. Each effect of two reasons is estimated.

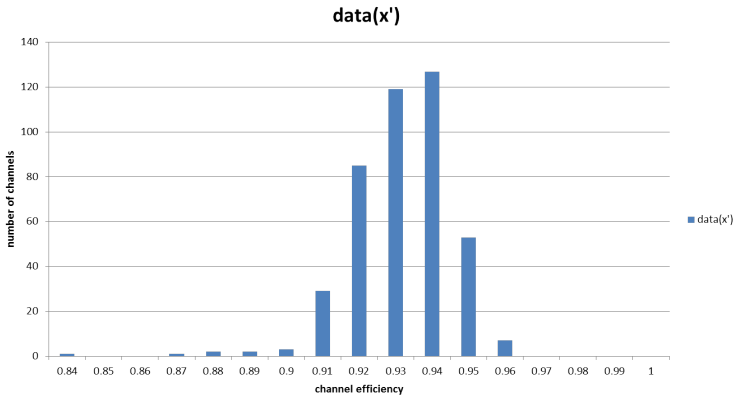

Figure 3.42: Distribution of channel efficiency of x'

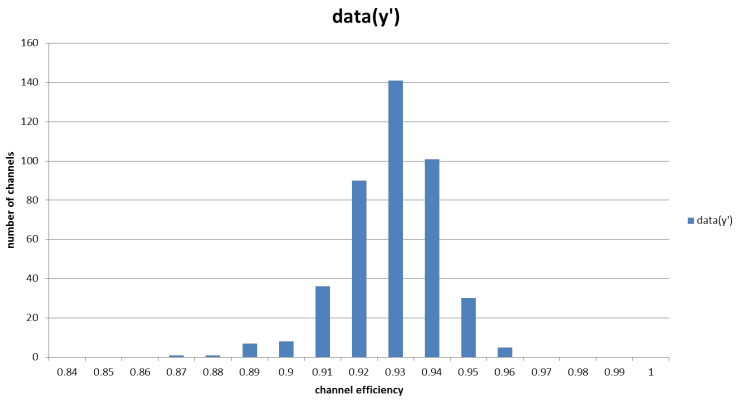

Figure 3.43: Distribution of channel efficiency of y'

To estimate inefficiency from charge distribution, average of charge in 2.5 p.e. – 40 p.e. of hits on straight track is calculated. To suppose charge distribution as Poisson distribution, fraction of 0, 1 and 2 p.e. is estimated. For example, in data of x', average of charge in 2.5 p.e. – 40 p.e. of hit is 13.3 p.e. and sum of fraction of 0, 1 and 2 p.e. estimated from Poisson distribution is 0.017%. It is much smaller compared to measured channel inefficiency.

The total width of layer 0 in x' is measured to be 52.3 $\pm$ 0.1 mm. A layer consists of 34 fibers (32 as tracker and two as mechanical space). A cross section of scintillating fiber shown in Fig. 3.44. Core is scintillating part and made of polystyrene (C_8H_8). Clad and Coat is not scintillating part and made of $C_5H_8O_2$ and TiO_2. Size of each part is shown below.

- $d_{fib} = 1.493 \pm 0.013[mm]$
- $d_{clad} = d_{fib} \times 0.02 \pm d_{fib} \times 0.002[mm]$
- $d_{all} = 1.520 \pm 0.016[mm]$

Ratio of scintillating part by size of a fiber tracker is $93.18 \pm 0.2[\%]$. It can explain channel efficiency of data.

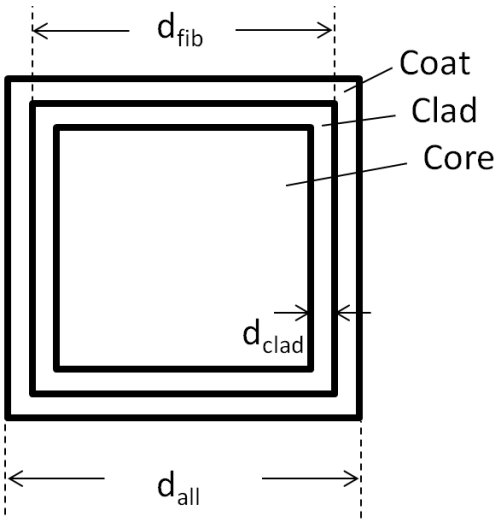

Figure 3.44: Section of scintillating fiber

As described in Sec. 3.2.1, layers are staggered by 0.5 channel. So a track is reconstructed even if there is inefficient channel. The track reconstruction efficiency is more than 99% in incident tracks.

Chapter 4

Event reconstruction and event selection

To select events with absorption and charge exchange, events without $\pi^{\pm}$ in the final state are searched for. In this chapter, the event reconstruction and selection are explained.

4.1 Event reconstruction

4.1.1 Overview of event reconstruction

To reconstruct events, following steps are taken. The detail of each step will be described in the following sections.

- Beam and hit selection
- Incident track search
- End point of the incident track
- Vertex finding
- Secondary track search
- Vertex position check in two dimensional views
- Matching between tracks x' and y'
- Particle identification with dE/dx

4.1.2 Beam and hit selection

First, initial π is selected by Cherenkov counter and time of flight as described in Sec. 3.1. The threshold of signal from PIAnO fiber is set at 2.5 p.e. If the signal of a hit is less than 10 p.e. and the adjacent hit on MAPMT has more than 20 p.e., the hit is considered as crosstalk and is not used in the reconstruction.

4.1.3 Incident track search

From incident track search to secondary track search, event on x' and y' are reconstructed independently.

In order to find the track of the incident particle, the number of hits along a virtual track is counted from upstream layer. When there are more than two channels without hits on the virtual track from start point (most upstream layer in this case), count is stopped. In this way of count is used when number of hits on tracks is counted. The position of the virtual track is scanned every 0.5 channel as shown in Fig. 4.1. The angle of the track is also changed from -4 degree to 4 degree by 1degree. The track with the largest number of hits is selected as incident track.

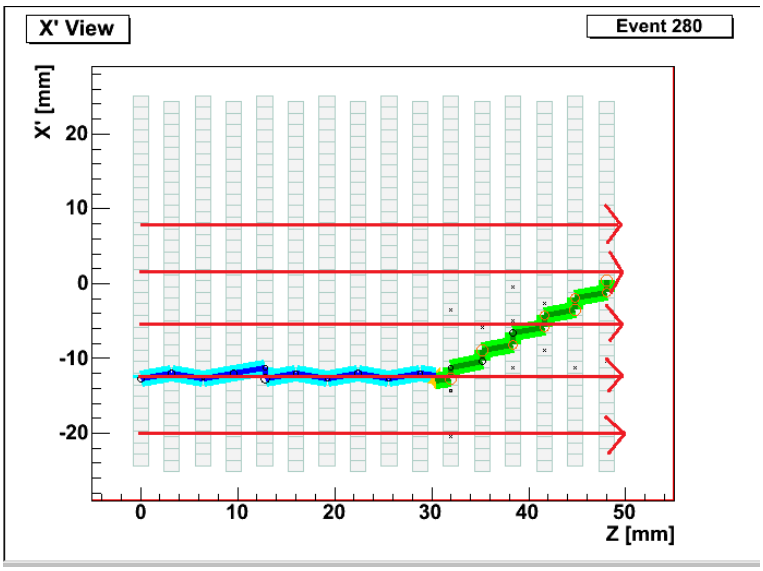

Figure 4.1: Searching incident track

4.1.4 End point of the incident track

End point of the incident track is searched for. If the signal of the most downstream hit of the incident track is more than 20 p.e., this point is removed from

the track. It is to distinguish secondary track of proton from incident track of π. Until there is a hit which is not removed with this condition, this condition of removal is repeated. Then the most downstream hit is defined as the end point of the incident track as Fig. 4.2.

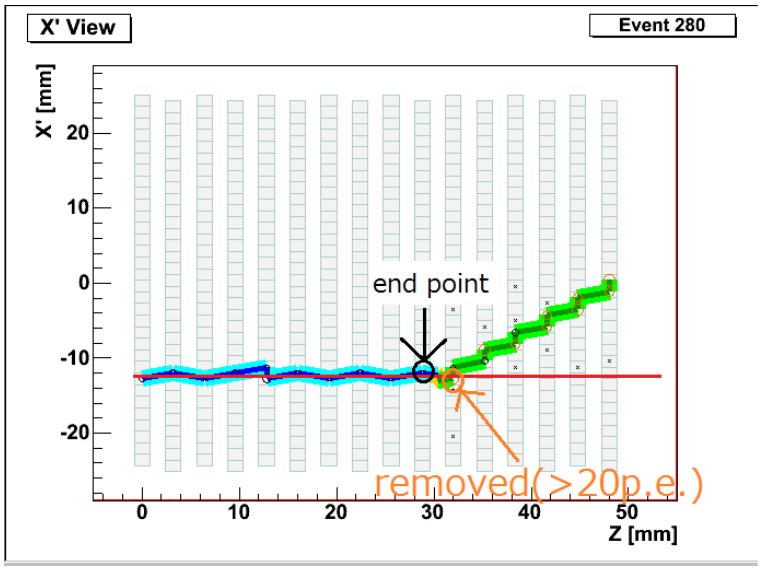

Figure 4.2: Searching the end point of the incident track

4.1.5 Vertex finding

The interaction vertex is searched for around the end point of the incident track. A vertex candidate position is scanned within +3/-2 channels in z in with 1 channel step and $\pm$ 1 channels in x' and y' with 0.5 channel step. From each position, straight lines are drawn to all the directions every one degree (Fig. 4.3). The number of lines with more than two hits, N_{track}, is counted. The total number of hits on the lines, N_{hit_total} is counted. Only line with more than two hits are included in counting N_{hit_total}. For channels which are used in N_{hit_total}, the sum of photoelectrons Q_{total} is calculated.

The vertex position is determined with the following criteria. If the first criterion is not met, second criterion is checked (and the third).

- Position with the largest N_{hit_total} is selected as a vertex. It is because the number of hits on tracks becomes largest at the true vertex.
- N_{hit_total} is the same, the position with the smallest N_{track} is selected as a vertex. In this case, if the number of tracks is smaller, each track has larger number of hits and misreconstruction is less likely.

- Position with largest Q_{total} is selected as a vertex. It is because larger charge is more likely to come from hit with a particle.
- Position nearest from the end of incident track is selected as a vertex.

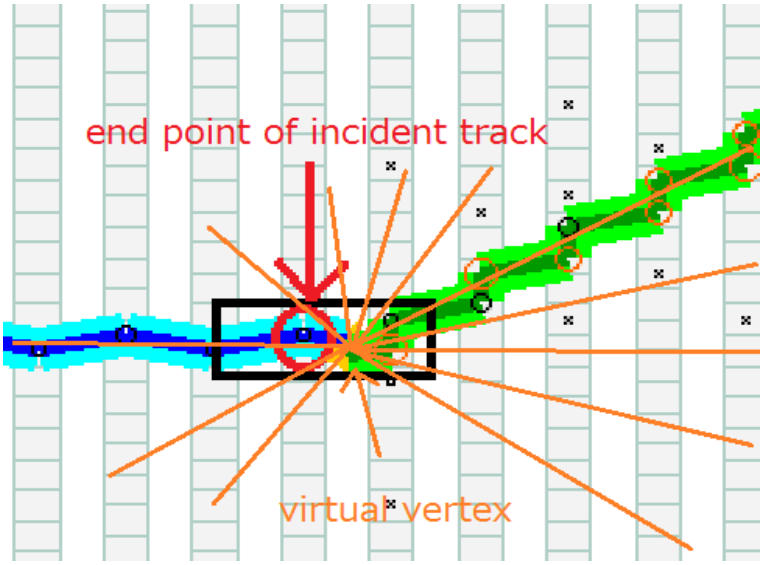

Figure 4.3: Searching vertex point

4.1.6 Secondary track search

From the vertex, virtual secondary tracks are drawn in all angles by 1 degree as shown in Fig. 4.4. Hits on the incident track are not used. The number of hits on virtual secondary track is counted. The track with the largest number of hits is selected as a secondary track if the number of hits is more than two. Then, hits on this track are removed and the same procedure is repeated. End points of the each track are defined as the most upstream and downstream hits.

4.1.7 Vertex position check in two dimensional views

Up to this point, the reconstruction is performed in two dimensional views. The z coordinate of vertex candidate in x' and y' is checked. If they are different by more than 2 channels, reconstruction is revised either in x' or y' . Which view is to be revised is selected with the following criteria. If the first criterion is not met, second criterion is checked (and then the third).

1. The number of hits not associated with any tracks, N_{NA} is compared. If difference of N_{NA} between x' and y' is more than three, the view with

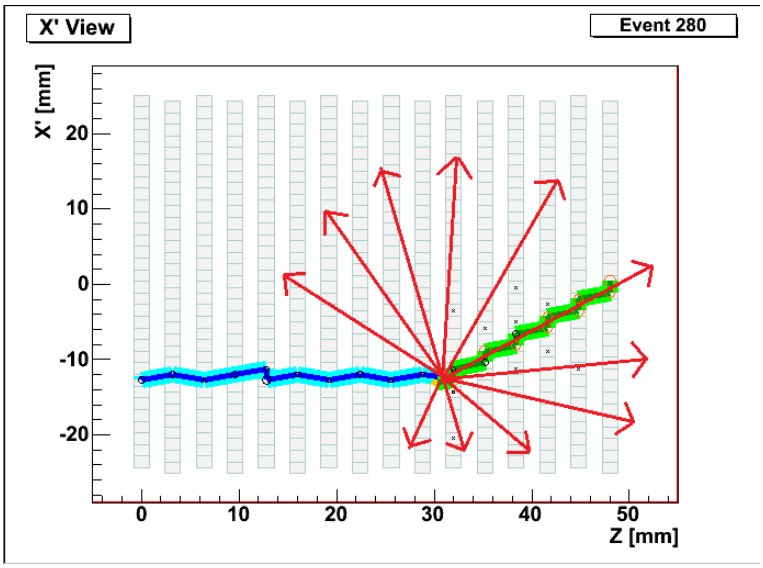

Figure 4.4: Searching secondary tracks

larger N_{NA} is selected. It is because the view with larger one has more possibility of misreconstruction.

2. If the number of tracks is different between x' and y', smaller one is selected. It is because the view with smaller one has more possibility of misconstruction.

3. If the number of tracks is the same in x' and y', the largest angle of tracks in x' and y' are compared. The view with smaller one is selected. It is because larger track is easier to detect vertex position.

Vertex position of z in the selected view is re-defined with the procedure described in Sec. 4.1.5 using vertex z in the other view as the starting point. The final vertex z position is an average of vertex z in x' and y' view after this process. Finally, reconstruction of secondary track is redone as described in Sec. 4.1.6

4.1.8 Matching between tracks x' and y'

3D tracks are reconstructed from two dimensional tracks. First, incident tracks of x' are matched with those of y' as 3D track. 2D angle of secondary tracks are calculated in x' and y'. Then combination of tracks in x' and y' are checked whether satisfying either of conditions below.

- The end points of tracks are in the fiducial volume and position of z of end point of tracks in x' and y' are within 2 channels.

- The end point of the track is out of the fiducial volume, scattering angle is less than 90 degree and the end point of the track is upstream within 2 channels or downstream of the end point of the track of the other projection.
- The end point of the track is out of the fiducial volume, scattering angle is more than 90 degree and the end point of the track is downstream within 2 channels or upstream of the end point of the track of the other projection.

If combinations of tracks satisfy this condition in a unique pattern, these secondary tracks of x' and y' are matched with each other as 3D tracks as shown in Fig. 4.5.

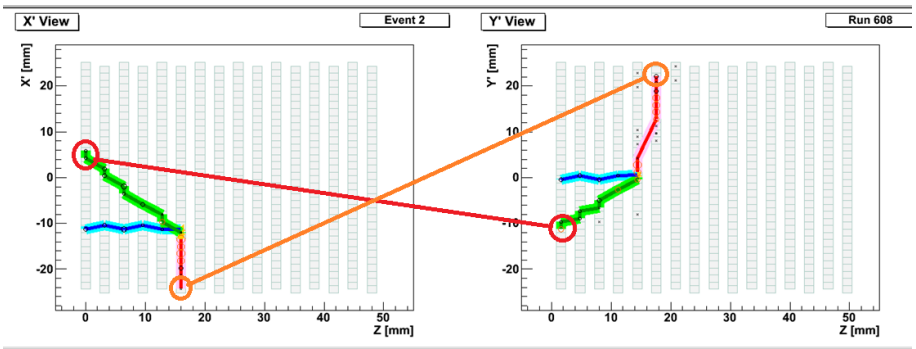

Figure 4.5: Secondary 3D track

If combinations of tracks satisfy this condition in several patterns, combination of tracks is determined with following criteria. If the first criterion is not met, second criterion is checked.

- Combination of tracks which has smallest difference of end point of tracks in x' and y' are matched.
- Combination of tracks which has smallest difference of energy deposit [p.e./mm] in x' and y' respectively are matched.

Figure 4.6 is an example of event display after reconstruction. Blue circles are signals under 20 p.e. and orange circles are signals over 20 p.e. Crosses are signals under 10 p.e. and adjacent hit in MAPMT is more 20 p.e., they are distinguished as crosstalk hits. Wider lines are reconstructed 2D tracks and thinner lines are reconstructed 3D tracks.

4.1.9 Particle identification with dE/dx

Figure4.7 shows energy deposit of secondary track in event whose scattering angle is within 30 degree. In absorption or charge exchange event, there is no

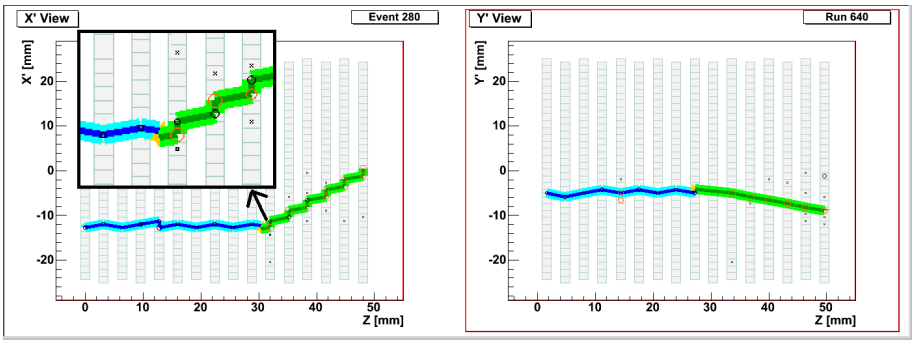

Figure 4.6: Reconstructed track

π after interaction. And in this case, particle of secondary track is proton. If event is cut in 12 p.e./mm, most of proton is not contained under 12 p.e./mm and is contained over 12 p.e./mm.

So energy deposit of tracks is calculated. Threshold is defined depending on the momentum of incident particles and angle of secondary tracks. Threshold of energy deposit of secondary track of 250 MeV/c is shown in Table 4.1. If energy deposit is smaller than threshold, its track is considered as π like track. If it is larger than threshold, its track is considered as proton like track.

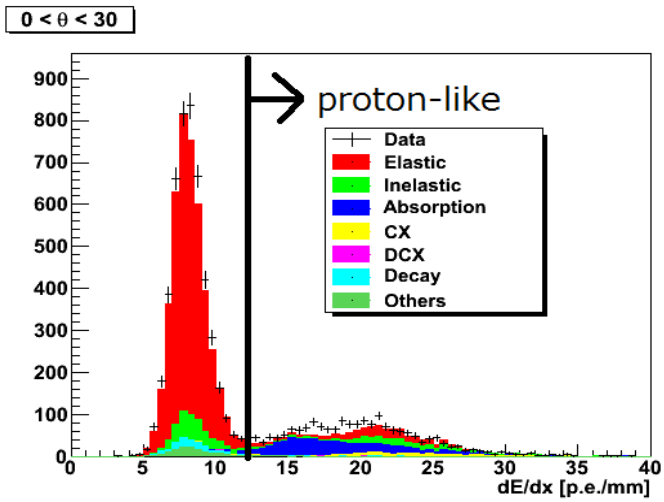

Figure 4.7: Energy deposit of secondary track and threshold of 12 p.e./mm

Example of a kind of track in event display is showed in Figure 4.8.

Table 4.1: Threshold of energy deposit of secondary track of 250 MeV/c

Angle of secondary track (degree)	Threshold of energy deposit (p.e./mm)
0 - 30	12
30 - 60	12.5
60 - 90	14
90 - 120	15
120 - 150	17
150 - 180	17

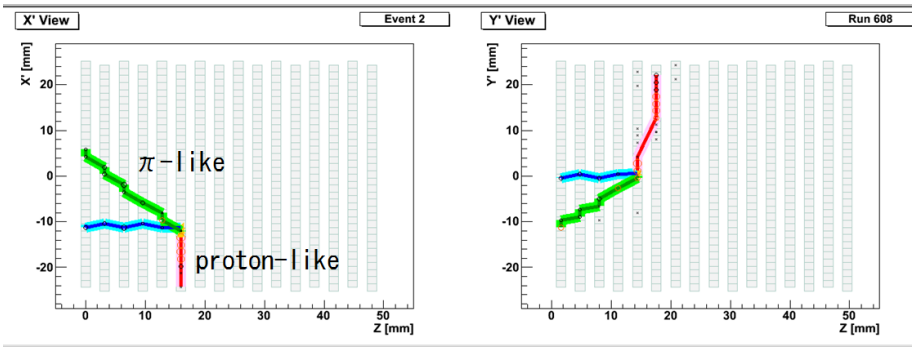

Figure 4.8: Event display after reconstruction

4.1.10 Vertex resolutions

To check whether vertex position is reconstructed well, reconstructed vertex position and true vertex position in MC is checked. Events after fiducial volume cut in Sec. 4.2.4 are used to select events with interaction. It is explained in detail in Sec. 4.2.4. Figure 4.9, 4.10 and 4.11 show differences of position between reconstructed vertex and real vertex in x, y and z in MC. Vertex position can be reconstructed within about 0.5 channels in x and y and about 1 channel in z. It indicates that vertex resolution is good enough compared with size of channel. Vertex resolution in x and y are better than one in z because incident π beam is horizontal.

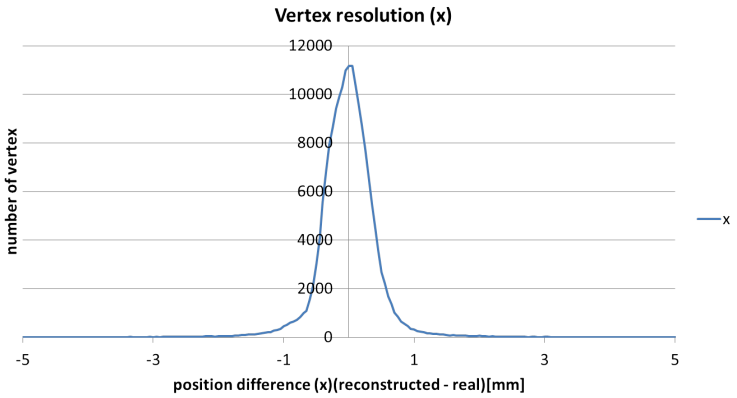

Figure 4.9: Vertex resolution of x

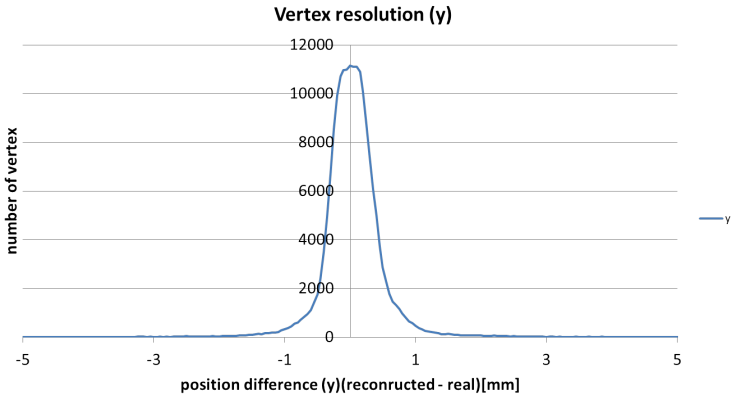

Figure 4.10: Vertex resolution of y

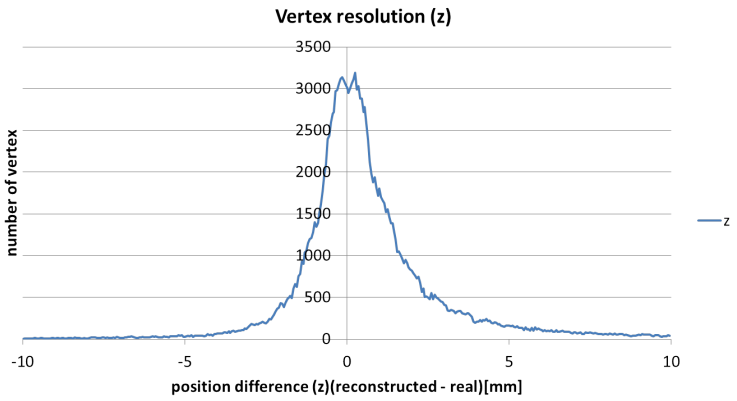

Figure 4.11: Vertex resolution of z

4.1.11 Secondary track efficiency

To check weather secondary track is reconstructed correctly, reconstructed secondary tracks are checked by real secondary tracks in MC by eye scan. Events after fiducial volume cut in Sec. 4.2.4 are used to select events with interaction. Tracks should be reconstructed with more than two hits, so less than real secondary track with less than three hits is removed from consideration. In 330 events, 300 events are reconstructed correctly.

9 events are reconstructed surplus in x' or y'.

- A track is reconstructed as two tracks as shown in Fig. 4.12(5 events)
- A track is reconstructed by mistake by multiple interaction (3 events)
- A track is reconstructed by mistake by other particles coming in (1 event)

15 events are reconstructed lack in x' or y'.

- A track is not reconstructed by near 90 degree scattering as shown in Fig.4.13(2 events)
- A track is not reconstructed by near 180 degree scattering (3 events)
- A track is not reconstructed by missing reconstruction of vertex position as shown in Fig 4.14(4 events)
- A track is not reconstructed by short proton track as shown in Fig. 4.15(5 events)
- 2D tracks are reconstructed correctly both x' and y', however tracks in x' and y' are not matched as 3D tracks. (1 event)

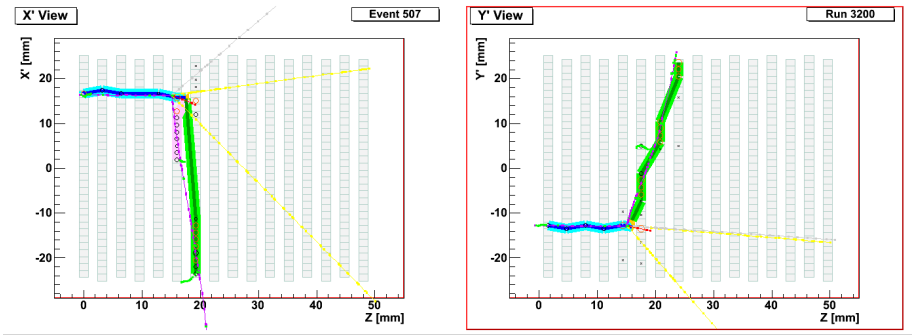

Figure 4.12: A track is reconstructed as two tracks

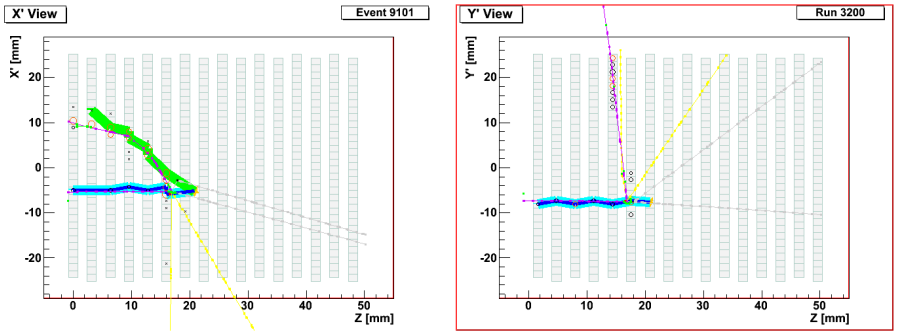

Figure 4.13: Near 90 degree scattering

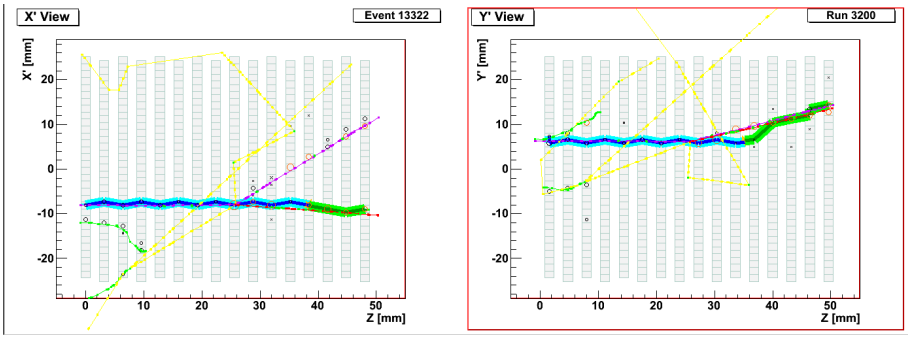

Figure 4.14: Missing reconstruction vertex position

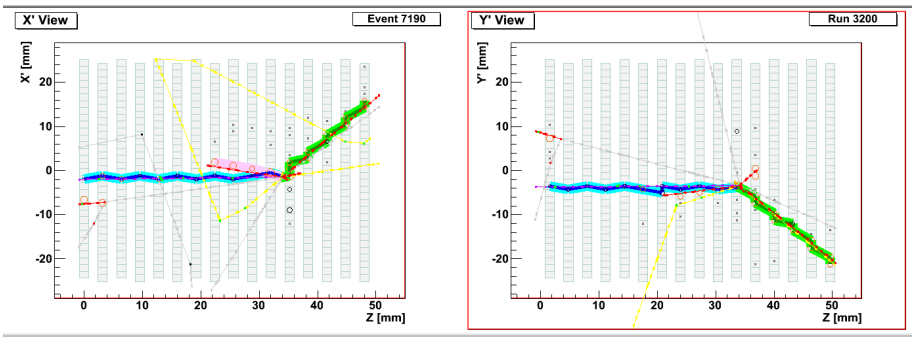

Figure 4.15: Short proton track

In 7 events, number of reconstructed tracks is same as real track, however reconstructed track is different from real track.

- Tracks in x' and y' is matched with opposite combination as 3D tracks as shown in Fig.4.16 (4 events)
- Other track is reconstructed by multiple interaction (1 event)
- Combination of hits on reconstructed tracks is different from real tracks as shown in Fig 4.17(2 event)

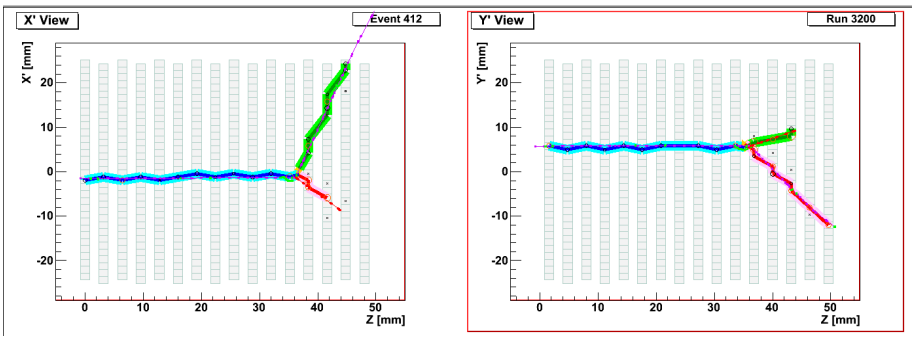

Figure 4.16: Tracks in x' and y' is matched with opposite combination as 3D tracks

About 91% of events with secondary tracks are reconstructed in this method.

4.1.12 Distributions of reconstructed variables

Number of reconstructed secondary tracks of data and MC after fiducial volume cut is showed in Figure 4.18. Each cut for event selection is explained in the

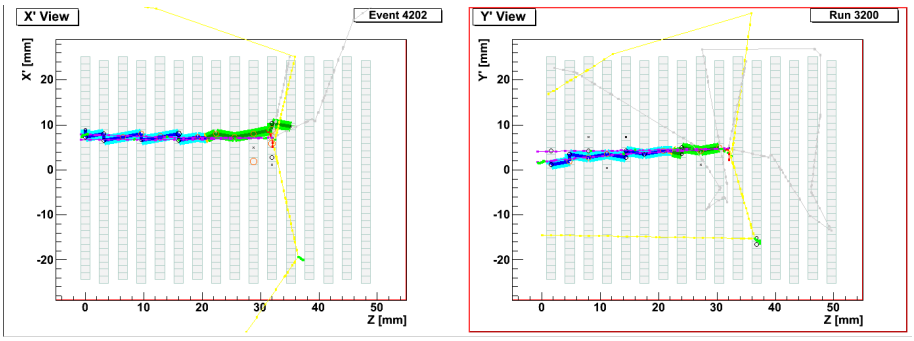

Figure 4.17: Combination of hits on reconstructed tracks is different from real tracks

next section.

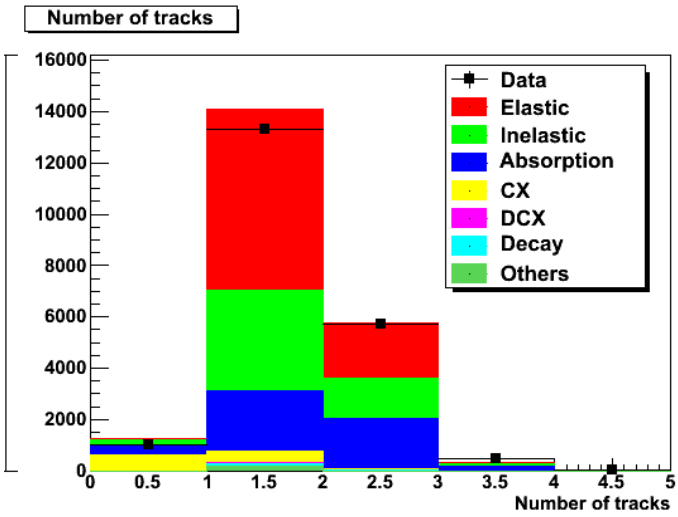

Figure 4.18: Number of secondary tracks of 250MeV/c

Number of reconstructed secondary 3D tracks of data and MC after fiducial volume cut is showed in Fig. 4.19. This is normalized the number of event after incident track quality cut. This 3D tracks is used to event selection in next section. From this figure in MC, about 1/4 of the event is absorption or charge exchange event. To select these events, event selection is explained in next section. A sum of events after fiducial volume cut in MC is 2% larger than data. Difference between data and MC comes from accuracy of tuning of MC.

Energy deposit of secondary track is shown in Fig. 4.20

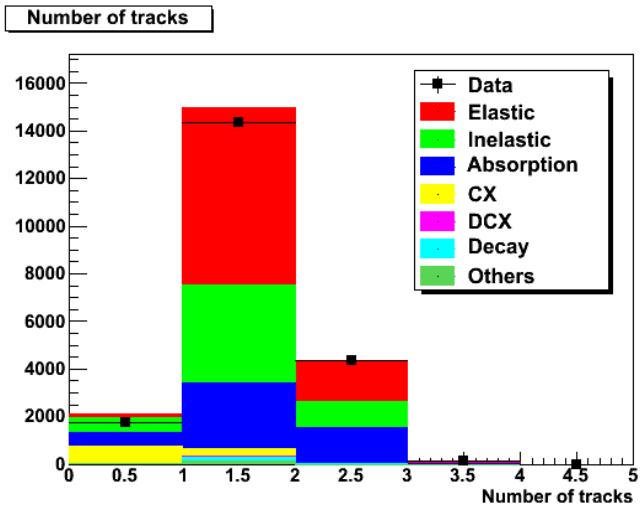

Figure 4.19: Number of secondary 3D tracks of 250MeV/c

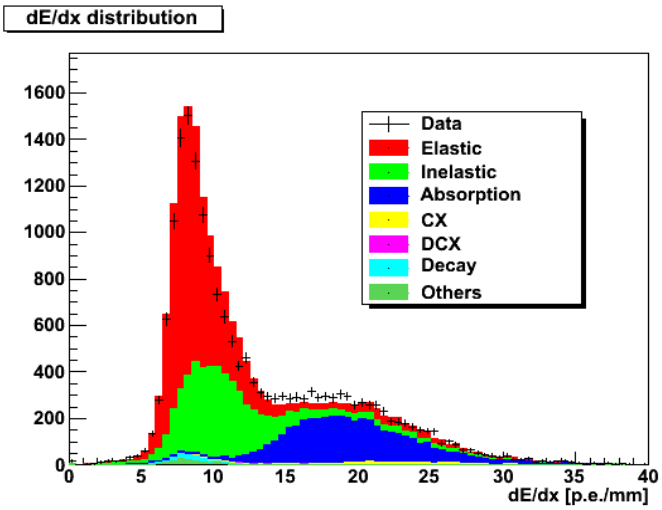

Figure 4.20: Distribution of energy deposit of secondary track of 250MeV/c

Vertex distribution of x and y of data and MC of 250MeV/c is shown in Fig. 4.21. Vertex distribution of z of data and MC of 250MeV/c is shown in Fig. 4.22

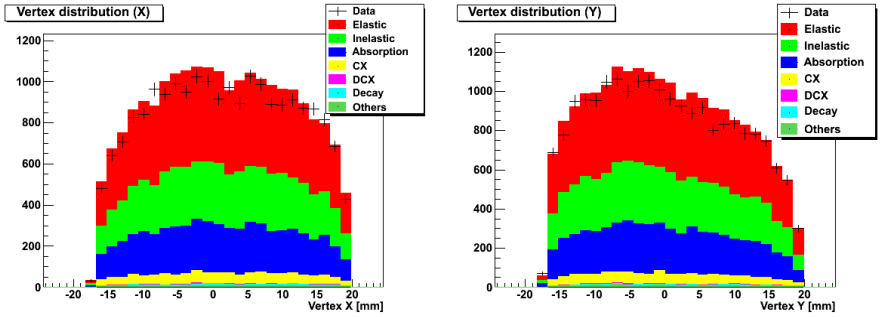

Figure 4.21: Vertex distribution of x and y of 250MeV/c

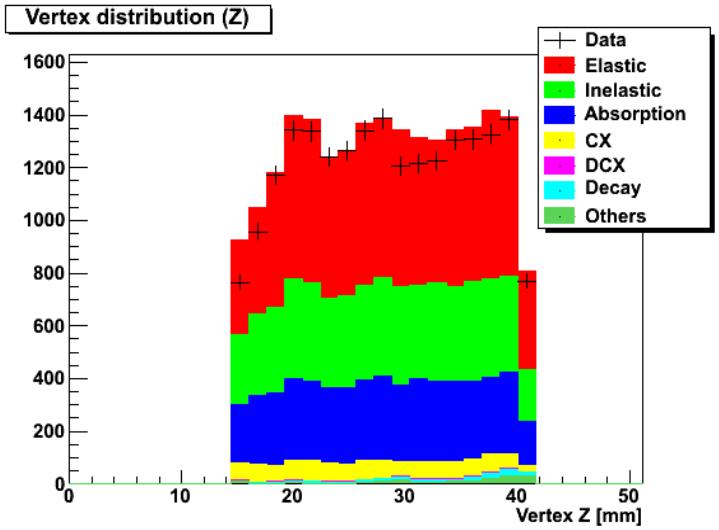

Figure 4.22: Vertex distribution of z of 250MeV/c

Angular distribution of secondary tracks of data and MC of 250MeV/c is shown in Fig. 4.23

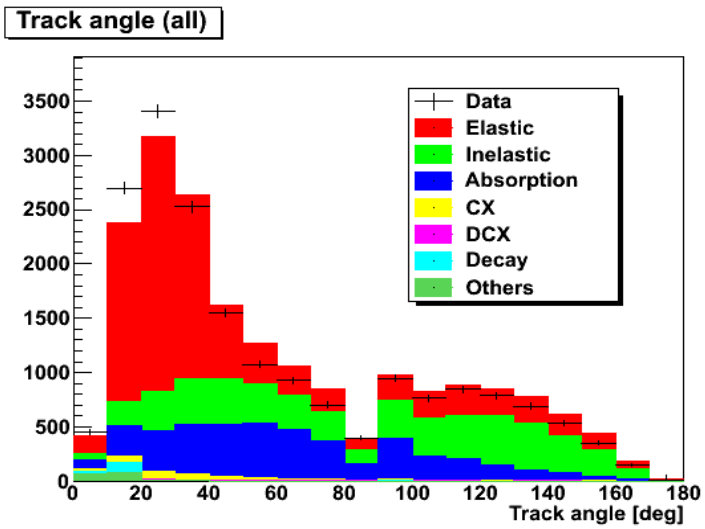

Figure 4.23: Angular distribution of secondary tracks of 250MeV/c

4.2 Event selection

4.2.1 Overview of event selection

To select absorption and charge exchange events, event selections of following steps are taken to select events without π^+ after interaction.

- Incident track quality (Incident track is checked whether it is horizontal)
- Multiple scattering cut (Low angle scattering event is cut)
- Fiducial volume cut (Vertex position is checked whether it is in the fiducial volume)
- Secondary track PID (Events without π^+ after interaction are selected)

4.2.2 Incident track quality

Hits are required in layer 0, 2 and 4 to select horizontal incident track as Fig. 4.24.

4.2.3 Multiple scattering cut

Most of multiple scattering is small angle. To remove multiple scattering events, small angle scattering events are removed if there are secondary tracks. First, two lines which are parallel to the incident track and apart by ± 2 channels are

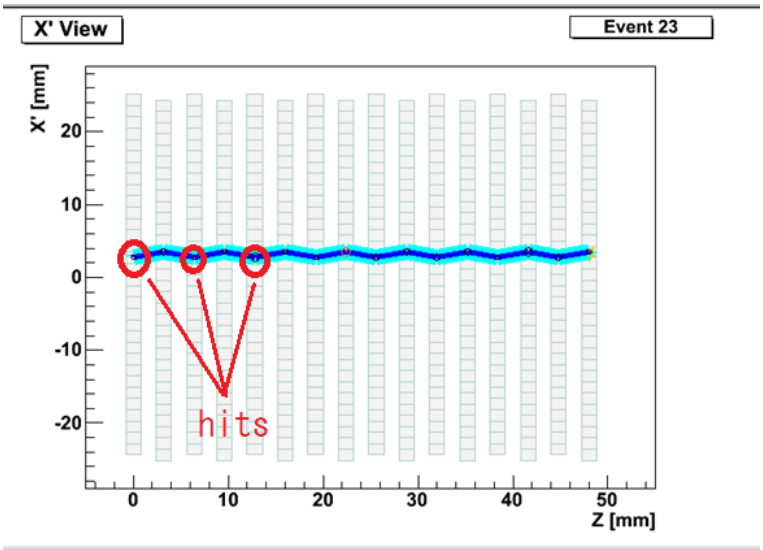

Figure 4.24: Required hits in layer 0, 2 and 4

drawn as shown in Fig. 4.25. If either of conditions below is satisfied, this event is removed.

- The sum of the number of reconstructed hits inside of two lines of x' and y' is more than 25.
- The sum of the number of reconstructed hits outside of two lines of x' and y' is 0.
- The number of hits in the most downstream three layers is more than one in both x' and y'.

Figure 4.26 is an example of rejected event as a multiple scattering event.

4.2.4 Fiducial volume cut

Figure 4.27 shows the distribution of the position of incident π. It is measured at the upstream surface of the detector. If interaction occurs near the edge of detector, the track of the particle may be short and it becomes hard to be reconstructed. So, a fiducial volume is set to remove these events. Fiducial volume in x and y is set as Figure 4.27.

- $-22.2 < x < 23.9$,
- $-16.1 < y < 22.8$,
- $-17.4 < (x - y)/\sqrt{2} < 19.7$

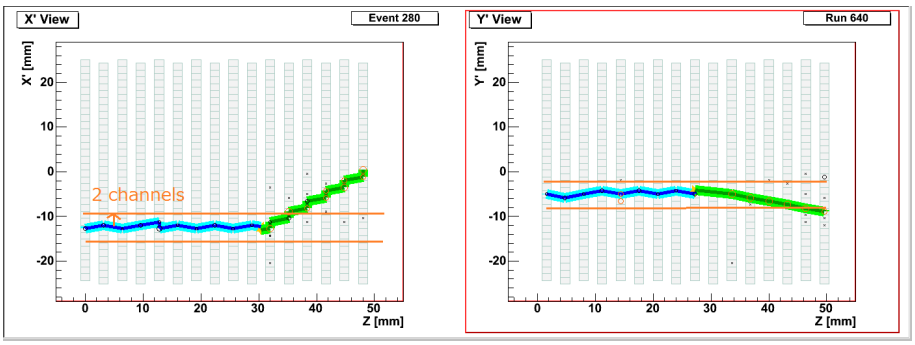

Figure 4.25: Example of event not rejected by multiple scattering event cut

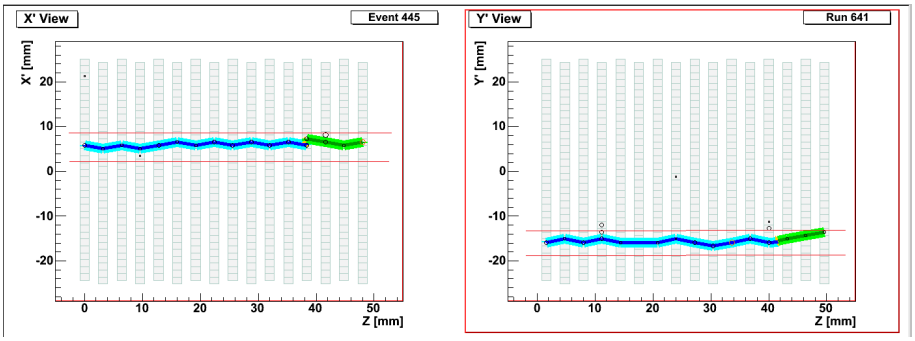

Figure 4.26: Example of an event rejected by multiple scattering event cut

- $-17.4 < (x+y)/\sqrt{2} < 19.7$

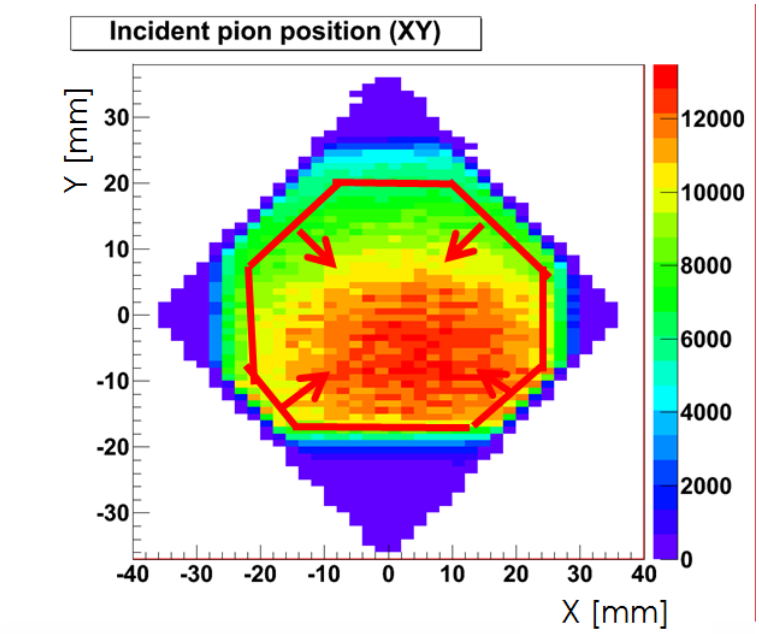

Figure 4.27: Position of incident π and fiducial volume cut of x and y

Figure 4.28 shows position of vertex in z of data of 250MeV/c. The red and black histograms show the distribution for the events with and without secondary track, respectively. Fiducial volume is set $13.8 < z < 40.5$ as shown in Figure 4.28. In upstream, it is hard to be reconstructed because hits in layer 0, 2, and 4 are required by good incident cut. In downstream, the number of end point through going event becomes large. It is because it is end on the way if there is inefficient channel in downstream. So upstream and downstream is cut as out of fiducial volume.

4.2.5 Secondary track PID

Event without π-like secondary track is chosen. Figure 4.29 is an example of event selected as absorption or charge exchange.

4.2.6 Summary of event selection

The event selection efficiency for absorption and charge exchange is about 74%. Number of event after cut of data and MC of 250MeV/c is shown in Table 4.2. Number of tracks and angular distribution after cut of data and MC is shown

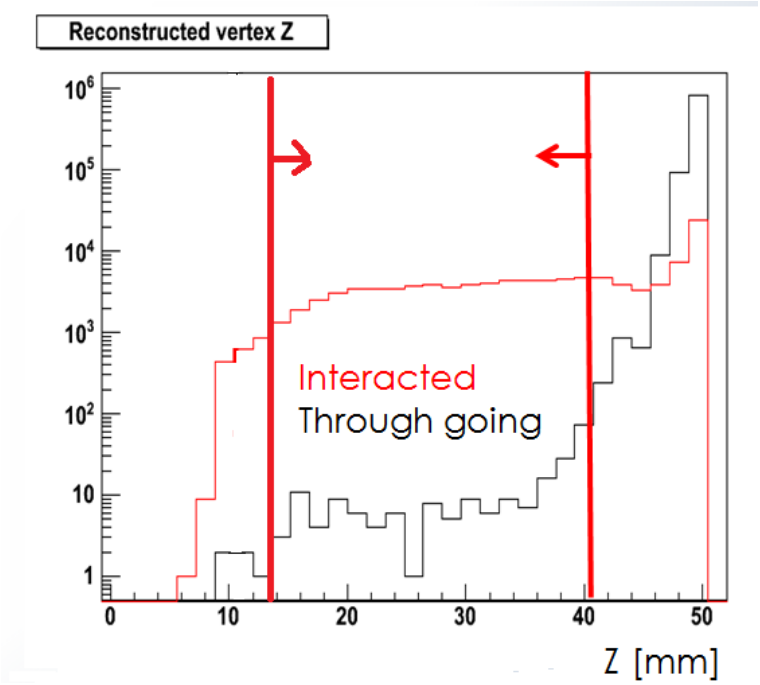

Figure 4.28: Vertex position or end point (through going) of z and fiducial volume cut of z

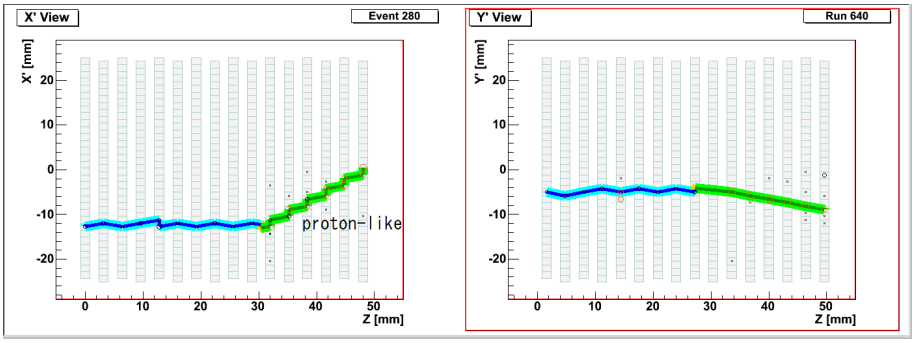

Figure 4.29: Selected event as absorption or charge exchange

in Figs. 4.30 and 4.31. Number of each type of event in MC after selection is shown in Table 4.3.

Table 4.2: Number of event after each cut in data and MC of 250MeV/c

Selection	Data	MC
S0 and S1 trigger and beam PID selection	872455	2508645
Incident track quality cut	259540	810456
Multiple scattering cut	42446	131558
Fiducial volume cut	20548	67079
Secondary track PID cut	7226	22292

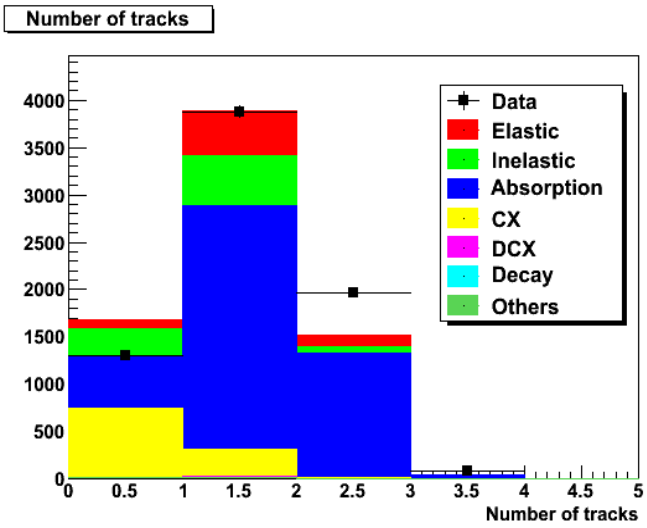

Figure 4.30: Number of 3D tracks after secondary track PID cut of 250MeV/c

Purity of absorption and charge exchange events is about 76.8%. Most of background is inelastic interaction.

4.3 Background estimation

Events after fiducial volume cut and not satisfying secondary track PID cut (π-like tracks are contained in secondary tracks) are called background samples. In the samples, most events are not absorption or charge exchange events. The background samples are used to check the background contamination in the final sample by comparing data and MC simulation. Using background samples,

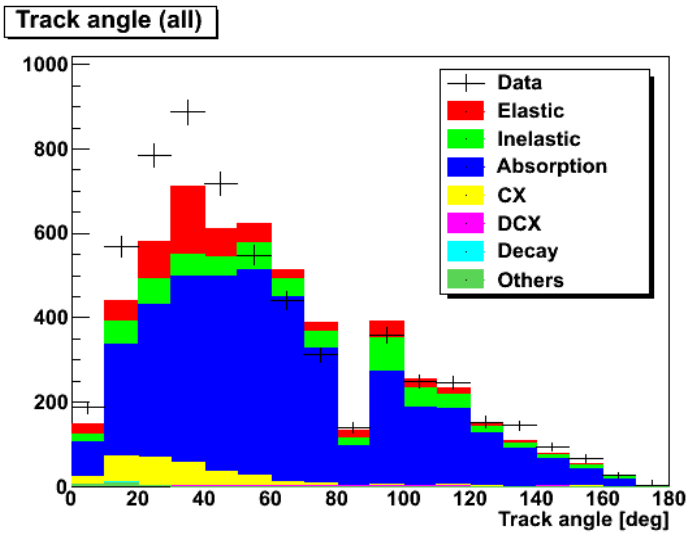

Figure 4.31: Angular distribution of tracks after secondary track PID cut of 250MeV/c

Table 4.3: The number of each kind of event in MC after selection of 250MeV/c

Event type in MC	Number of events	Fraction (%)
Absorption	13933	62.5
Charge exchange	3179	14.3
Elastic	2199	9.9
Inelastic	2791	12.5
Double charge exchange	78	0.3
Decay	23	0.1
Others	89	0.4

uncertainty of background events which is not absorption and charge exchange event after selection is estimated in Sec. 5.3.

Number of 3D matched tracks and angular distribution of tracks in back ground samples are shown in Figs. 4.32 and 4.33. The background samples contain absorption and charge exchange events of about 3%.

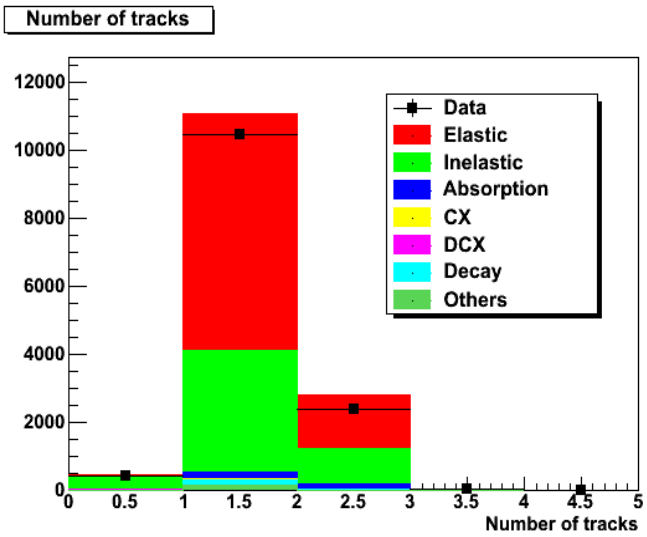

Figure 4.32: Number of 3D tracks in background samples of 250MeV/c

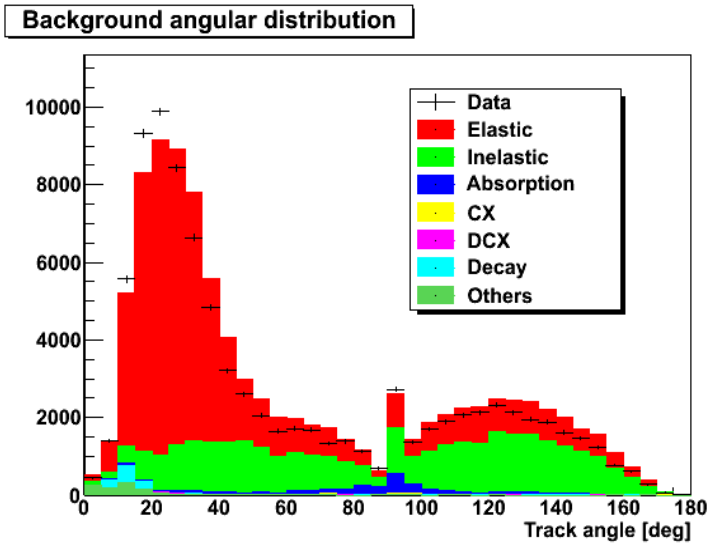

Figure 4.33: Angular distribution of tracks in background samples of 250MeV/c

Chapter 5

Systematic error

In this chapter, systematic error of cross section is estimated. The following sources are considered.

- Signal efficiency
- Vertex resolution in fiducial volume
- Background estimation
- Charge distribution
- Crosstalk rate
- Fiber alignment
- Channel efficiency
- μ/e contamination
- Beam momentum
- Beam profile
- Number of target nuclei

5.1 Uncertainties of signal efficiency

Three sources are considered for uncertainties of signal efficiency.

- Model uncertainty of the secondary particles
- Secondary track PID

5.1.1 Model uncertainty of the secondary particles

The uncertainty in modeling the angular distribution of the secondary particles in signal events may affect the reconstruction efficiency. Angular distributions of the secondary track with smallest angle in the final sample for data and MC simulation are shown in Fig. 5.1. The uncertainty is estimated by reweighting the angular distribution of the MC simulation so that the number of forward- and backward-going tracks match to data, as shown in Fig 5.2. The difference of the efficiency between nominal and reweighting MC simulation is 1.38%. It is assigned as the systematic uncertainty.

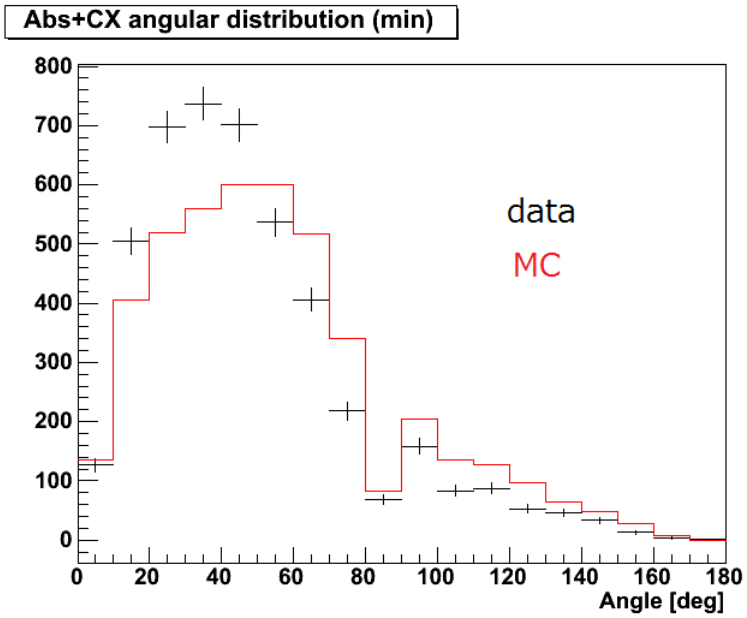

Figure 5.1: Angular distribution of the secondary tracks with smallest angle in the final event sample

5.1.2 Secondary track PID cut efficiency

The uncertainty of particle identification of secondary track affects the efficiency. Based on the eye scan of remaining events, four reasons of PID failure are identified; dE/dx resolution (65.8%), gamma conversion (25.3%), crosstalk fake track (3.7%) and high momentum p (5.2%). Uncertainty of each source is estimated as follows.

- The inefficiency of PID is estimated by calculating dE/dx in x and y views independently and looking at the other view. The uncertainty from dE/dx

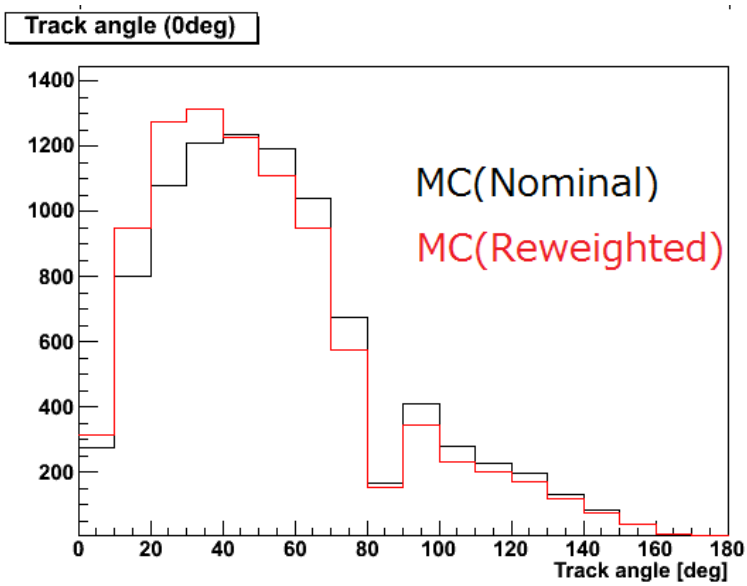

Figure 5.2: Angular distribution of the secondary tracks in the final event sample of nominal MC and reweighted MC

resolution is estimated from the difference of PID inefficiency between data and MC simulation.

- Conversion of gamma near the vertex can produce a fake secondary track. Figure 5.3 shows an example of gamma conversion. Error from the gamma conversion is estimated by comparing gamma conversion probability in default Geant4 and EPDL (Evaluated Photon Data Library by Lawrence Livermore National Laboratory)[13].
- The uncertainty from the crosstalk fake track is included in the systematic error crosstalk, which is described later.
- Error from high momentum protons is estimated by the difference of high momentum proton events from Geant4 and NEUT.

In total the uncertainty of signal efficiency is estimated to be 2.33%.

5.2 Vertex resolution in fidutial volume

If the vertex resolution is different between data and MC simulation, the number of events after selection after fiducial volume cut changes. The uncertainty is estimated by the difference of efficiency with several definition of the fiducial volume as shown in Fig. 5.4. The uncertainty is estimated to be 1.87%.

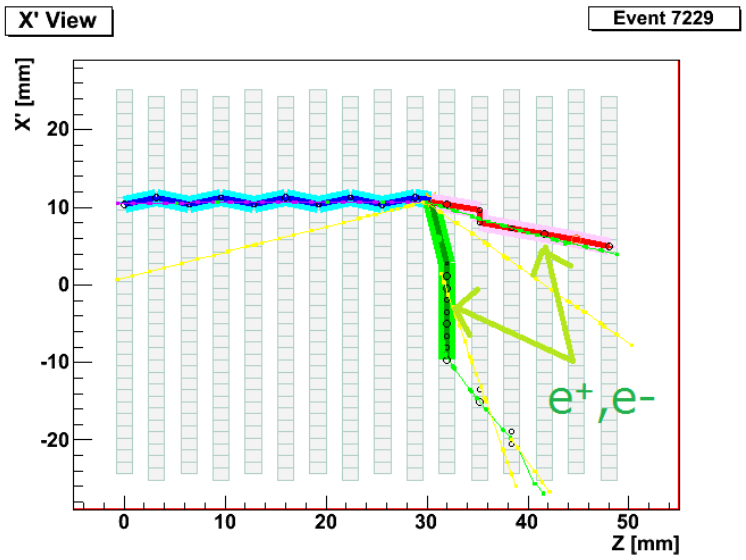

Figure 5.3: Event with gamma conversion

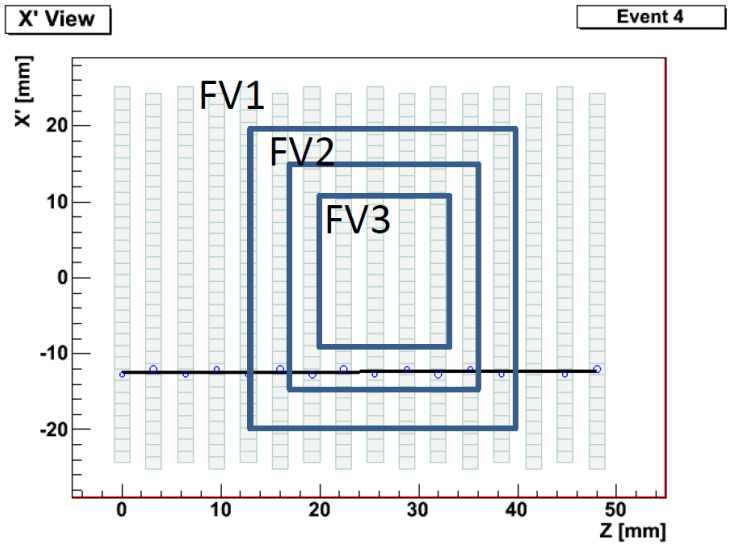

Figure 5.4: Changing fiducial volume

5.3 Uncertainties of background estimation

Two sources are considered for the uncertainties of the background estimation.

- Scattering model uncertainty
- Impurity of background samples

5.3.1 Scattering model uncertainty

The uncertainty of scattering model affects the number of background events after selection. Based on eye scan of background sample which is required π-like track after interaction, four reasons of failure of scattering event selection are identified; π reconstruction failure (37.3%), multiple interaction (32.6%), dE/dx resolution (24.3%) and low momentum π (5.8%). Uncertainty for each source is estimated as follows.

- The uncertainty of number of π reconstruction failure and dE/dx resolution failure are estimated together by comparing the number of background samples in data and MC simulation. Figure 5.5 shows an example of π not being reconstructed. Purple line shows a real track of π.
- The uncertainty of number of background samples from multiple interaction is estimated from number of each type of multiple interaction events and cross section uncertainty from past data of Ashery [2].
- Error from low momentum π is estimated from difference of fraction of under 135 MeV/c of inelastic scattering π in Geant4 and NEUT.

5.3.2 Impurity of background samples

If fraction of absorption and charge exchange event in background samples are different between data and MC simulation, background event changes. The uncertainty is estimated from uncertainty of number of absorption and charge exchange event in background samples from absorption and charge exchange cross section uncertainty of past data of Ashery [2].

In total, the uncertainty of background estimation is -3.57/+2.41%.

5.4 Uncertainty of charge distribution

The charge from MAPMT is used to define a hit and to distinguish π-like track and proton-like track. In MC simulation, there are three parameters to control charge distribution; 1 p.e. resolution, energy to p.e. conversion factor, and non-linearity correction. Comparing, shape of charge distribution of data and MC simulation, uncertainty of parameters are estimated. Fluctuated these parameters within these uncertainties, the charge in cross section is estimated. Uncertainty is estimated to be 0.46%.

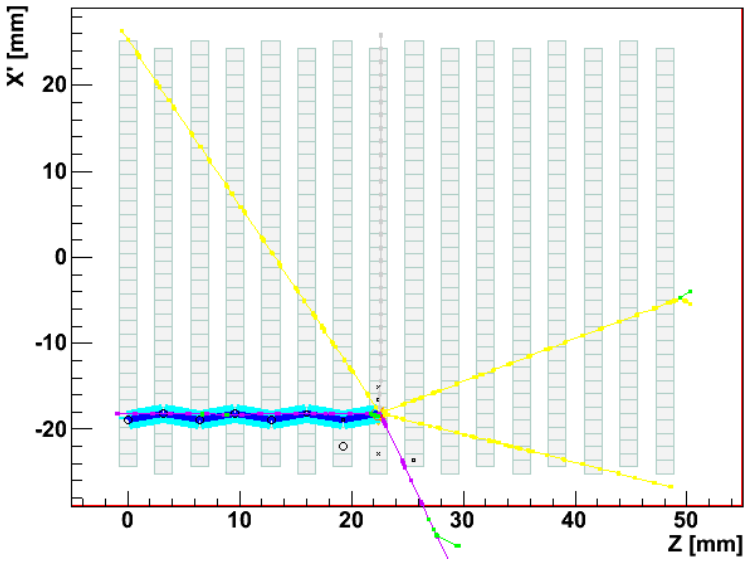

Figure 5.5: Event with π not being reconstructed

5.5 Uncertainty of crosstalk rate

If crosstalk rate changes, reconstruction miss by crosstalk hit changes. What is more, if signal of secondary track is piled up from crosstalk from the other tracks, secondary track PID is changed. Crosstalk rate has eight parameters of adjacent channels in MAPMT explained in Sec.3.3.1. Crosstalk rate of tuned and upper limit and lower limit of each channel is estimated as shown in Tables 3.3, 3.4 and 3.5. Cross sections of three MC whose crosstalk rate is tuned, upper limit and lower limit are compared. Uncertainty is estimated to be 0.53%.

5.6 Uncertainty of fiber alignment

If fiber alignment is different, vertex position is changed and the number of event after fiducial volume cut is changed. Fiber alignment is fluctuated in error and change of cross section is estimated as uncertainty. Uncertainty is estimated to be 0.82%.

5.7 Uncertainty of channel efficiency

If channel efficiency is changed, reconstruction of tracks is changed. Difference of channel efficiency of data and MC simulation is defined as error. Hits are removed with the error randomly and cross section is calculated. Uncertainty is estimated to be 0.76%.

5.8 μ/e contamination

The uncertainty of μ/e contamination affects of number of interaction event. This uncertainty has two causes. First one is uncertainty of beam purity estimated from Cherenkov counter and TOF. Second one is π beams decay between S0 and a fiber tracker. Probability of π^+ decays between S0 and a fiber tracker is 0.89% and this is much larger than first one. Therefore, uncertainty of μ/e contamination is estimated to be 0.89%.

5.9 Uncertainty of beam momentum

The uncertainty of beam momentum affects cross section of interaction. Beam momentum and its error are calculated by Harpsichord range measurement. Error of momentum is about 1MeV/c. Uncertainty of cross section is estimated by difference of cross section of MC with fluctuated momentum in error. Systematic error is estimated to be 1.34%

5.10 Uncertainty of beam profile

The uncertainty of beam profile affects incident π quality. In beam profile, beam position and angle are contained. Uncertainty of beam position and angle is estimated from comparing one measured from PIAnO and true one. Systematic error is estimated from cross section by fluctuated these parameters in uncertainty. Systematic error is estimated to be 1.55%.

5.11 Uncertainty of number of target nuclei

Uncertainty of number of target nuclei affects number of interaction events. Number of target nuclei is estimated from size of scintillating fiber and density. From uncertainty of size and density, uncertainty of number of target nuclei is estimated. Uncertainty of number of target nuclei is estimated to be 0.86%.

5.12 Summary of the systematic errors

All the systematic errors are summarized in Table 5.1. The total systematic error is 5.40%.

Table 5.1: Summary of all the systematic errors

Error source	systematic error
Signal efficiency	2.33%
Vertex resolution in fiducial volume	1.87%
Background estimation	-3.57/2.41%
Charge distribution	0.46%
Crosstalk rate	0.53%
Fiber alignment	0.82%
Channel efficiency	0.76%
μ/e contamination	0.89%
Beam momentum	1.34%
Beam profile	1.55%
Number of target nuclei	0.86%
Total	-5.40/+4.71%

Chapter 6

Measurement of cross section

The cross section is calculated from the number of events after the selection, N_{sel}^{data}. The number of background events (N_{BG}) is estimated with the MC simulation. The number of event with the interaction in TiO_2 coating in data ($N_{TiO_2}^{data}$) is estimated from past experiment [11] [12]. The number of MC events is normalized to the number of events for data after the incident track quality cut. In the MC simulation, the true particle ID information of the secondary tracks is checked. The number of events with no π^+ in the secondary track, N_{absCX}^{MC}, is counted. The number of event with the interaction in TiO_2 coating in MC ($N_{TiO_2}^{MC}$) is counted from true information. The fraction of π^+ (f_π) is estimated by the beamline detectors and correction in the cross section calculation as

$$\sigma_{data} = \sigma_{MC} \times \frac{N_{sel}^{data} - N_{BG} - N_{TiO_2}^{data}}{N_{absCX}^{MC} - N_{TiO_2}^{MC}} \times \frac{1}{f_\pi}. \tag{6.1}$$

In the denominator, the true absorption and charge exchange events after the selection for MC simulation are counted. In the numerator, events after the selection of data after selection and background subtraction are counted.

The number used to calculate the cross section are listed in Table 6.1.

The cross section for 250MeV/c π^+ is calculated as Eq. (6.1).

$$\sigma_{data} = 214.43 \times \frac{7226.00 - 1658.84 - 347.39}{5479.94 - 346.33} \times \frac{1}{0.9957} \tag{6.2}$$

$$= 218.97 \pm 3.7(stat.)[mbarn] \tag{6.3}$$

Cross section of the π^+ absorption and charge exchange with ^{12}C is measured to be

$$218.97 \pm 3.7(stat.) - 11.8/ + 10.3(syst.)[mbarn]. \tag{6.4}$$

Table 6.1: Value of each parameter

Parameter	Value of each parameter
$\sigma_{MC}[mbarn]$	214.43
N_{sel}^{data}	7226.00
N_{BG}	1658.84
$N_{TiO_2}^{data}$	347.39
N_{absCX}^{MC}	5479.94
$N_{TiO_2}^{MC}$	346.33
f_π	0.9957

Chapter 7

Conclusion

In T2K experiment, neutrino oscillation is studied. Main signal of neutrino interaction is ($\nu_\ell + n \to \ell + p$), and background signal is ($\nu_\ell + N \to \ell + N' + \pi$). Sometimes π is absorbed into nucleus and background event cannot be distinguished from main signal. This is one of large systematic error of the experiment. However, cross section of π absorption into nucleus has 20 – 30 % error in past experiment. Reduction of this systematic error is our goal. Cross section of π^+ absorption and charge exchange into nucleus is measured and cross section of charge exchange is measured by γ rays from π^+ by NaI measurement. In this thesis, measurement of cross section of π absorption and charge exchange into ^{12}C for 250MeV/c is presented.

In our measurement, detector called PIAnO is used. PIAnO is made of 1024 scintillating fibers, 32 channels in a layer and 32 layers arranged in orthogonal directions alternately to reconstruct 3D tracks of charged particles. In data taking, π^+ beam from M11 beamline in TRIUMF is used. Data of Run 1 (150, 375 MeV/c of π^+ with scintillation target) are taken in 2010. Data of Run 2 (200, 275 and 325 MeV/c of π^+ with water target) are taken in 2011. First, channel efficiency of fiber tracker of PIAnO is measured to know detector performance. Using hits on through going track, channel efficiency is measured to be 93.19 $\pm$ 0.04 (92.90 $\pm$ 0.04) in x' (y').

Then crosstalk rate of MC is tuned with number of channel with 2.5 p.e. – 5 p.e. in adjacent channels of hits on tracks in MAPMT. Uncertainty of crosstalk rate is estimated. The uncertainty of cross section from crosstalk rate is measured to be 0.53%. Total systematic error of cross section is 5.40%.

Then cross section of π^+ absorption and charge exchange into ^{12}C is measured. To select absorption and charge exchange events, events without π-like tracks in secondary tracks are selected. Comparing data and MC, cross section of absorption and charge exchange is measured.

Cross section of π^+ absorption and charge exchange into ^{12}C for 250 MeV/c is measured to be

$$218.97 \pm 3.7(stat.) - 11.8/ + 10.3(syst.)[mbarn]. \tag{7.1}$$

We plan to measure the cross section with other momentum of π^+ and cross section with water target, which is the material used for super-Kamiokande. Also, the measurement of cross section of π^+ absorption into nucleus is ongoing by using NaI to reduce systematic error of analysis of neutrino oscillation in T2K.

Bibliography

[1] Z. Maki, M. Nakagawa and S. Sakata, "Remarks on the unified model of elementary particles," Prog. Theor. Phys. **28**, 870 (1962).

[2] D. Ashery, I. Navon, G. Azuelos, H. K. Walter, H. J. Pfeiffer and F. W. Schleputz, "True Absorption And Scattering Of Pions On Nuclei," Phys.Rev.C **23**, 2173 (1981).

[3] P. de Perio, "NEUT pion FSI," AIP Conf. Proc. **1405**, 223 (2011).

[4] H.Q.Ingram et al. "Interaction Effects in $^{16}O(\pi^{\pm}, \pi^{\pm}p)^{15}N$ and Δ-Nucleus Interactions," Phys.Rev.C27 1578 (1983)

[5] Y. Hayato, "NEUT," Nucl. Phys. Proc. Suppl. **112**, 171 (2002).

[6] G. Mitsuka, "NEUT," AIP Conf. Proc. **981**, 262 (2008).

[7] Salceo et al. "Computer Simulation Of Inclusive Pion Nuclear Reaction," Nucl.Phys.A484 577 (1988)

[8] K. Nitta et al. "The K2K SciBar Detector," Nucl.Instrum.Meth.A 535 147 (2004)

[9] "Reference Physics List," http://geant4.cern.ch/support/proc_mod_catalog-/physics_lists/referencePL.shtml, accessed in January 5, 2013

[10] H.L.Anderson et al. "Total Cross Section for Nagative and Positive Pion in Hydron and Deutrium," Phys.Rev.96 1104 (1954)

[11] D.Ashery, "Pion nucleus Reactions," Nucl.Phys.A35 555C-576C (1988)

[12] K.Nakai et al."Measurements of Cross Sections for Pion Absorption by Nuclei," Phys.Rev.Lett.44 1446-1449 (1980)

[13] G.A.P.Cirrone et al. "Validation of the Geant4 electromagnetic photon cross-sections for elements and compounds," Nucl.Instrum.Meth.A618 (2010) 315-322